Eur. Phys. J. C (2021) 81:169
https://doi.org/10.1140/epjc/s10052-021-08944-w

THE EUROPEAN PHYSICAL JOURNAL C

Regular Article - Theoretical Physics

Cosmic inflation in minimal $U(1)_{B-L}$ model: implications for (non) thermal dark matter and leptogenesis

Debasish Borah[1,a], **Suruj Jyoti Das**[1,b], **Abhijit Kumar Saha**[2,c]

[1] Department of Physics, Indian Institute of Technology Guwahati, Guwahati, Assam 781039, India
[2] Theoretical Physics Division, Physical Research Laboratory, Navrangpura, Ahmedabad 380009, India

Received: 20 August 2020 / Accepted: 3 February 2021 / Published online: 18 February 2021

Abstract We study the possibility of realising cosmic inflation, dark matter (DM), baryon asymmetry of the universe (BAU) and light neutrino masses in non-supersymmetric minimal gauged $B-L$ extension of the standard model with three right handed neutrinos. The singlet scalar field responsible for spontaneous breaking of $B-L$ gauge symmetry also plays the role of inflaton by virtue of its non-minimal coupling to gravity. While the lightest right handed neutrino is the DM candidate, being stabilised by an additional Z_2 symmetry, we show by performing a detailed renormalisation group evolution (RGE) improved study of inflationary dynamics that thermal DM is generally overproduced due to insufficient annihilations through gauge and scalar portals. This happens due to strict upper limits obtained on gauge and other dimensionless couplings responsible for DM annihilation while assuming the non-minimal coupling to gravity to be at most of order unity. The non-thermal DM scenario is viable, with or without Z_2 symmetry, although in such a case the $B-L$ gauge sector remains decoupled from the inflationary dynamics due to tiny couplings. We also show that the reheat temperature predicted by the model prefers non-thermal leptogenesis with hierarchical right handed neutrinos while being consistent with other requirements.

1 Introduction

Precision measurements of the cosmic microwave background (CMB) anisotropies by experiments like Planck [1–3] reveal that our universe is homogeneous and isotropic on large scales upto a remarkable accuracy. However, the observed isotropy of the CMB leads to the horizon problem which remains unexplained in the standard cosmology where the universe remains radiation dominated throughout the early stages. In order to solve the horizon problem, the presence of a rapid accelerated expansion phase in the early universe, called inflation [4–6] was proposed. Originally proposed to solve the horizon, flatness and unwanted relic problems in standard cosmology, the inflationary paradigm was also subsequently supported by the adiabatic and scale invariant perturbations observed in the CMB [1,2]. Such an early accelerated phase of expansion can be generated by the presence of one or more scalar fields whose dynamics crucially decides the period of inflation. Over the years, a variety of inflationary models have been studied with different levels of success [7]. The earliest proposal of this sort is known as chaotic inflation [8,9] where simple power law potentials like $m^2\phi^2$ with a scalar field ϕ were used. However, such simple models predict very specific values of inflationary parameters like the spectral index $n_s \sim 0.967$, tensor-to-scalar ratio $r \sim 0.133$ for number of e-folds $N_e = 60$ and unfortunately, the latest Planck 2018 data [2] strongly disfavour this simple model due to its large prediction of r. Modified chaotic inflation where the inflation sector is extended by an additional scalar field to assist the inflaton field has also been proposed [10–12]. Another class of models use the Higgs as the inflaton [13,14]. These models often suffer from problems of vacuum stability [15] and non-unitarity [16] as well as being inadequate for combining inflation with other cosmological problems like DM and BAU. A possible way out is to consider a beyond standard model (BSM) singlet scalar which acts as the inflaton. We consider this possibility in our

During the review process of this manuscript, the affiliation of Abhijit Kumar Saha has been changed to "School of Physical Sciences, Indian Association for the Cultivation of Science, 2A and 2B Raja S.C. Mullick Road, Kolkata 700 032". The new institutional email address of AKS is "psaks2484@iacs.res.in".

[a] e-mail: dborah@iitg.ac.in (corresponding author)
[b] e-mail: suruj@iitg.ac.in
[c] e-mail: aks@prl.res.in

work where an additional scalar with non-minimal coupling to gravity [17–20], in addition to usual quartic chaotic type coupling, can give rise to successful inflation while predicting the inflationary parameters within the observed range. The same scalar field is also responsible for several other interesting phenomenology as we discuss below.

The same CMB measurements mentioned above also suggest that the present universe has a significant amount of non-luminous, non-baryonic form of matter, known as dark matter (DM) [3,21]. This is also supported by astrophysical evidences gathered over a much longer period of time [22–24]. The Planck 2018 data reveals that approximately 26% of the present universe is composed of DM, which is about five times more than the ordinary luminous or baryonic matter. In terms of density parameter $\Omega_{\rm DM}$ and h = Hubble Parameter/(100 km s^{-1}Mpc^{-1}), the present DM abundance is conventionally reported as [3]: $\Omega_{\rm DM}h^2 = 0.120 \pm 0.001$ at 68% CL. Since none of the standard model (SM) particles can satisfy the criteria of a particle DM candidate, several proposals have been put forward among which the weakly interacting massive particle (WIMP) is perhaps the most popular one. In this framework, a DM particle having mass and interactions typically around the electroweak scale can give rise to the observed DM abundance after thermal freeze-out, a remarkable coincidence often referred to as the *WIMP Miracle* [25]. The same interactions responsible for thermal freeze-out of WIMP type DM should also give rise to sizeable DM-nucleon scattering. However, null results at direct detection experiments like LUX [26], PandaX-II [27,28], XENON1T [29,30] have certainly pushed several WIMP models into a tight corner, if not ruled out yet. This has also generated interests in beyond thermal WIMP paradigms as viable alternatives. One such interesting possibility is the non-thermal origin of DM [31]. For a recent review of such feebly interacting (or freeze-in) massive particle (FIMP) DM, please see [32]. In the FIMP scenario, DM candidate does not thermalise with the SM particles in the early universe due to its feeble interaction strength and the initial abundance of DM is assumed to be zero. At some later stage, DM can be produced non thermally from decay or annihilation of other particles thermally present in the universe.

Similarly, the baryonic content of the universe also gives rise to another puzzle due to the abundance of baryons over antibaryons. Quantitatively, this excess is denoted as baryon to entropy ratio [3,21]

$$Y_B = \frac{n_B - n_{\bar{B}}}{s} = (8.24 - 9.38) \times 10^{-10} \quad (1)$$

where Y_B denotes comoving baryon density, $n_B\,(n_{\bar{B}})$ denotes baryon (anti-baryon) number density while s is the entropy density. Since any initial asymmetry before inflation will be washed out at the end of inflation due to the exponential expansion of the universe, there has to be a dynamical mechanism to generate the asymmetry in a post-inflationary universe. This requires certain conditions, known as the Sakharov conditions [33] to be fulfilled. They are namely, baryon number (B) violation, C and CP violation and departure from thermal equilibrium, not all of which can be fulfilled in the required amounts within the SM alone. Generation of baryon asymmetry of the universe (BAU) from out-of-equilibrium decays of heavy particles has been a well-known mechanism for baryogenesis [34,35]. Another interesting way, which also connects the lepton sector physics, is known as leptogenesis, proposed a few decades back [36]. In leptogenesis, instead of creating a baryon asymmetry directly from B violating interactions, an asymmetry in lepton sector is created via lepton number (L) violating processes (decay or scattering). If this lepton asymmetry is generated before the electroweak phase transition (EWPT), then the $(B + L)$-violating electroweak sphaleron transitions [37] can convert it to the required baryon asymmetry. Since the quark sector CP violation is insufficient to produce the required baryon asymmetry, the mechanism of leptogenesis can rely upon lepton sector CP violation which may be quite large as hinted by some neutrino oscillation experiments [38,39]. An interesting feature of this scenario is that the required lepton asymmetry can be generated through CP violating out-of-equilibrium decays of the same heavy fields that take part in popular seesaw mechanisms [40–45] which also explains the origin of tiny neutrino masses [21], another observed phenomena which the SM fails to address.

Motivated by these, we study a minimal extension of the SM, by a gauged $B - L$ symmetry with three right handed neutrinos (RHN) required to cancel the anomalies and a singlet scalar to break the additional gauge symmetry spontaneously while simultaneously generating RHN masses. Although previously analysed separately, the consistency of these three entities together have not been examined in this simple kind of BSM setup before as per our knowledge. We also perform a complete RG evolution of all the relevant couplings to determine the fate of the scenarios we discuss here. While in this framework, the singlet scalar plays the role of inflation, one RHN is stabilised by an additional Z_2 symmetry to become a DM candidate. The other two RHNs can give rise to light neutrino masses with vanishing lightest neutrino mass apart from producing the required lepton asymmetry which gets converted into the observed baryon asymmetry via sphalerons. Interestingly, we find that the stringent limits on the inflationary observables from Planck 2018 and BICEP 2/Keck Array (BK15) data [2] as well as the stability of inflaton potential restrict the $B - L$ gauge coupling, scalar couplings and Yukawa couplings associated with the inflaton field to be within some limits which do not favour thermal DM scenario due to insufficient annihilations. As an alternative, with very tiny gauge and Yukawa couplings, one can realise the non-thermal DM scenario (with or with-

out Z_2 symmetry) while the inflationary potential behaviour merges with the usual case of quartic inflation with non minimal coupling to gravity. We also find that the predicted values of reheat temperature makes it difficult to realise high scale thermal N_2 leptogenesis [46,47] with hierarchical RHN leaving the option of non-thermal leptogenesis [48–56] viable.

The structure of the paper is organised as follows. In Sect. 2, we discuss the particle content of the proposed setup and their interactions followed by brief mention of the existing constraints in Sect. 3. In Sect. 4 we perform a detailed study of inflation and its predictions in view of Planck 2018 bounds. We discuss different aspects of DM phenomenology in Sect. 5 and then move onto discussing the possibility of non-thermal leptogenesis in Sect. 6. Finally we conclude in Sect. 7.

2 The model

As mentioned earlier, we study a gauged $B-L$ extension of the SM with the minimal field content which can give rise to cancellation of triangle anomalies, spontaneous gauge symmetry breaking, light neutrino masses, dark matter, leptogenesis and cosmic inflation. While gauged $B-L$ extension of the SM was proposed long ago [57–62], realising a stable DM candidate in the model requires non-minimal field content or additional discrete symmetries. Also, a gauged $B-L$ model with just SM fermion content, is not anomaly free due to the non-vanishing triangle anomalies for both $U(1)^3_{B-L}$ and mixed $U(1)_{B-L}-(\text{gravity})^2$ anomalies. These triangle anomalies for the SM fermion content are given as

$$\begin{aligned}&\mathcal{A}_1\left[U(1)^3_{B-L}\right]=\mathcal{A}_1^{\rm SM}\left[U(1)^3_{B-L}\right]=-3\,,\\&\mathcal{A}_2\left[(\text{gravity})^2\times U(1)_{B-L}\right]\\&\quad=\mathcal{A}_2^{\rm SM}\left[(\text{gravity})^2\times U(1)_{B-L}\right]=-3\,.\end{aligned}\tag{2}$$

Remarkably, if three right handed neutrinos with $B-L$ charge -1 each are added to the model, they contribute $\mathcal{A}_1^{\rm New}\left[U(1)^3_{B-L}\right]=3, \mathcal{A}_2^{\rm New}\left[(\text{gravity})^2\times U(1)_{B-L}\right]=3$ leading to vanishing amount of triangle anomalies. This is perhaps the most economical setup of anomaly cancellation and hence we adopt it here.[1] To have a stable DM candidate we introduce a discrete Z_2 symmetry under which one of the RHN is odd whereas all other fields are even. In Tables 1 and 2, we have listed all fermions as well as scalar fields (including the SM ones) of the present model and their charges under the $SU(3)_c\times SU(2)_L\times U(1)_Y\times U(1)_{B-L}$ symmetry.

[1] For other exotic solutions to anomaly cancellation conditions, see [63–69].

Table 1 Fermion fields of the model and their corresponding gauge charges

Particles	$SU(3)_c\times SU(2)_L\times U(1)_Y\times U(1)_{B-L}$	Z_2
$q_L=\begin{pmatrix}u_L\\d_L\end{pmatrix}$	$(3,2,\frac{1}{6},\frac{1}{3})$	+
u_R	$(3,1,\frac{2}{3},\frac{1}{3})$	+
d_R	$(3,1,-\frac{1}{3},\frac{1}{3})$	+
$\ell_L=\begin{pmatrix}\nu_L\\e_L\end{pmatrix}$	$(1,2,-\frac{1}{2},-1)$	+
e_R	$(1,1,-1,-1)$	+
N_{R_1}	$(1,1,0,-1)$	−
N_{R_2}	$(1,1,0,-1)$	+
N_{R_3}	$(1,1,0,-1)$	+

Table 2 Scalar fields of the model and their corresponding gauge charges

Particles	$SU(3)_c\times SU(2)_L\times U(1)_Y\times U(1)_{B-L}$	Z_2
$H=\begin{pmatrix}H^+\\H^0\end{pmatrix}$	$(1,2,\frac{1}{2},0)$	+
Φ	$(1,1,0,2)$	+

The gauge invariant Lagrangian of the model is

$$\mathcal{L}=\mathcal{L}_{\rm SM}-\frac{1}{4}B'_{\alpha\beta}\,B'^{\alpha\beta}+\mathcal{L}_{\rm scalar}+\mathcal{L}_{\rm fermion}\,.\tag{3}$$

where $\mathcal{L}_{\rm SM}$ denotes the SM Lagrangian involving quarks, gluons, charged leptons, left handed neutrinos and electroweak gauge bosons while the second term is the kinetic term of $B-L$ gauge boson (Z_{BL}) expressed in terms of field strength tensor $B'^{\alpha\beta}=\partial^\alpha Z^\beta_{BL}-\partial^\beta Z^\alpha_{BL}$. The gauge invariant scalar Lagrangian of the model is as follows

$$\mathcal{L}_{\rm scalar}=(D_\mu H)(D_\mu H)^\dagger+(D_\mu\Phi)(D^\mu\Phi)^\dagger-V(H,\Phi)\,,\tag{4}$$

where

$$\begin{aligned}V(H,\Phi)=&-\mu_1^2|H|^2-\mu_2^2|\Phi|^2+\lambda_1|H|^4+\lambda_2|\Phi|^4\\&+\lambda_3|H|^2|\Phi|^2.\end{aligned}\tag{5}$$

The covariant derivatives of scalar fields are

$$D_\mu H=\left(\partial_\mu+i\frac{g_1}{2}\sigma_a W^a_\mu+i\frac{g_2}{2}B_\mu\right)H,\tag{6}$$

$$D_\mu\Phi=\left(\partial_\mu+i2g_{BL}Z_{BL\mu}\right)\Phi,\tag{7}$$

with g_1 and g_2 being the gauge couplings of $SU(2)_L$ and $U(1)_Y$ respectively and $W^a_\mu\,(a=1,\,2,\,3)$ and B_μ are the corresponding gauge fields. On the other hand Z_{BL}, g_{BL} are the gauge boson and gauge coupling respectively for $U(1)_{B-L}$ gauge group.

The gauge invariant fermionic Lagrangian of the model is as follows

$$\begin{aligned}\mathcal{L}_{\text{fermion}} = & \, i \sum_{\kappa=1}^{3} \overline{N_{R_\kappa}} \not{D} \left(Q_\kappa^R\right) N_{R_\kappa} \\ & - \sum_{j=2}^{3} \sum_{\alpha=e,\mu,\tau} Y_D^{j\alpha} \, \overline{l_L^\alpha} \tilde{H} N_R^j \\ & - \sum_{i=2}^{3} \sum_{j=2}^{3} Y_{N_{ij}} \Phi \, \overline{N_{R_i}^C} N_{R_j} \\ & - Y_{N_1} \Phi \, \overline{N_{R_1}^C} N_{R_1} + \text{h.c.} \end{aligned} \tag{8}$$

The covariant derivative is defined as

$$\not{D}(Q_\kappa^R) \, N_{R_\kappa} = \gamma^\mu \left(\partial_\mu + i g_{BL} \, Q_\kappa^{(R)} \, Z_{BL\mu}\right) N_{R_\kappa}, \tag{9}$$

with $Q_\kappa^R = -1$ being the $B - L$ charge of right handed neutrino N_{R_κ}. Due to the presence of Z_2 symmetry, N_{R_1} has no mixing with $N_{R_{2,3}}$ and also does not interact with SM leptons thereby qualifying for a stable DM candidate.

After breaking of both $B - L$ symmetry and electroweak symmetry by the vacuum expectation values (VEVs) of H and Φ, the form of doublet and singlet scalar fields are given by,

$$H = \begin{pmatrix} H^+ \\ \dfrac{h + v + iA}{\sqrt{2}} \end{pmatrix}, \quad \Phi = \frac{\phi + v_{BL} + iA'}{\sqrt{2}} \tag{10}$$

where v and v_{BL} are VEVs of H and Φ respectively. The right handed neutrinos and Z_{BL} get masses after the $U(1)_{B-L}$ breaking as,

$$M_{Z_{BL}} = 2 g_{BL} v_{BL}, \tag{11}$$

$$M_{N_i} = \sqrt{2} Y_{N_i} v_{BL}. \tag{12}$$

Here we consider diagonal Yukawa Y_N in $(N_{R_1}, N_{R_2}, N_{R_3})$ basis. Using Eqs. (11) and (12), it is possible to relate $M_{Z_{BL}}$ and M_{N_i} by,

$$M_{N_i} = \frac{1}{\sqrt{2} g_{BL}} Y_{N_i} M_{Z_{BL}}. \tag{13}$$

Also after the breaking of $SU(2)_L \times U(1)_Y \times U(1)_{B-L}$, the scalar fields h and ϕ can be related to the physical mass eigenstates H_1 and H_2 by a rotation matrix as,

$$\begin{pmatrix} H_1 \\ H_2 \end{pmatrix} = \begin{pmatrix} \cos\theta & -\sin\theta \\ \sin\theta & \cos\theta \end{pmatrix} \begin{pmatrix} h \\ \phi \end{pmatrix}, \tag{14}$$

where the scalar mixing angle θ is represented by

$$\tan 2\theta = -\frac{\lambda_3 v v_{BL}}{\left(\lambda_1 v^2 - \lambda_2 v_{BL}^2\right)}. \tag{15}$$

The physical scalar masses are given by,

$$M_{H_1}^2 = 2\lambda_1 v^2 \cos^2\theta + 2\lambda_2 v_{BL}^2 \sin^2\theta - 2\lambda_3 v v_{BL} \sin\theta \cos\theta, \tag{16}$$

$$M_{H_2}^2 = 2\lambda_1 v^2 \sin^2\theta + 2\lambda_2 v_{BL}^2 \cos^2\theta + 2\lambda_3 v v_{BL} \sin\theta \cos\theta. \tag{17}$$

Here M_{H_1} is identified as the SM Higgs mass whereas M_{H_2} is the singlet scalar mass.

One of the strong motivations of the minimal $U(1)_{B-L}$ model is the presence of heavy RHNs which can yield correct light neutrino mass via type I seesaw mechanism. The analytical expression for the light neutrino mass matrix is

$$m_\nu = m_D^T M_N^{-1} m_D, \tag{18}$$

where $m_D = Y_D v/\sqrt{2}$. We consider the right handed neutrino mass matrix M_N to be diagonal. Since in our case N_{R_1} does not interact with SM leptons, the lightest active neutrino would be massless. The Dirac neutrino Yukawa matrix Y_D can be formulated through the Casas–Ibarra parametrisation [70] as

$$Y_D = \sqrt{2} \frac{\sqrt{M_N}}{v} \mathcal{R} \sqrt{m_\nu^d} \, U_{\text{PMNS}}^\dagger, \tag{19}$$

where m_ν^d, M_N are the diagonal light and heavy neutrino mass matrices respectively and U_{PMNS} is the usual Pontecorvo–Maki–Nakagawa–Sakata (PMNS) leptonic mixing matrix. In the diagonal charged lepton basis, the PMNS mixing matrix is also the diagonalising matrix of light neutrino mass matrix

$$m_\nu = U_{\text{PMNS}}^* m_\nu^d U_{\text{PMNS}}^\dagger.$$

In the above Casas–Ibarra parametrisation, $\mathcal{R}$ represents a complex orthogonal matrix ($\mathcal{R}\mathcal{R}^T = \mathcal{I}$). In case of only two right handed neutrinos, the $\mathcal{R}$ matrix is a function of only one complex rotation parameter $z = z_R + i z_I, z_R \in [0, 2\pi], z_I \in \mathbb{R}$ [71]. For three right handed neutrinos taking part in seesaw mechanism $\mathcal{R}$ can depend upon three complex rotation parameters. Assuming one of them (rotation in 1–2 sector) to be vanishing, it can be represented as[2]

$$\mathcal{R} = \begin{pmatrix} \cos\gamma' & 0 & \sin\gamma' \\ -\sin\gamma\sin\gamma' & \cos\gamma & \sin\gamma\cos\gamma' \\ -\cos\gamma\sin\gamma' & -\sin\gamma & \cos\gamma\cos\gamma' \end{pmatrix}. \tag{20}$$

Therefore with suitable choices of γ and γ', the Yukawa matrix can take different forms. Here it remains pertinent

[2] For some recent discussions on choice of $\mathcal{R}$ matrix in the context of thermal and non-thermal dark matter as well as leptogenesis, please see [47].

to note that for a Z_2 symmetric Lagrangian ($\gamma' \sim 0$) as described in Eq. (8), the Dirac Yukawa coupling Y_D represents a 2×3 matrix in flavour basis. We shall use the best fit values of all three mixing angles and the mass squared differences of active neutrinos assuming a normal ordering [21].

3 Constraint on the model parameters

In this section, we briefly discuss the theoretical and experimental constraints on different parameters of the model.

To begin with, we consider the bounded from below criteria of the scalar potential. This gives rise to the following conditions to be satisfied by the quartic couplings,

$$\lambda_{1,2,3} \geq 0,\ \lambda_3 + \sqrt{\lambda_1 \lambda_2} \geq 0$$

. On the other hand, to avoid perturbative breakdown of the model, all dimensionless couplings must obey the following limits at any energy scale:

$$|\lambda_{1,2,3}| < 4\pi,\ |Y_D, Y_N| < \sqrt{4\pi},\ |g_1, g_2, g_{BL}| < \sqrt{4\pi}.$$

The non-observation of the extra neutral gauge boson in the LEP experiment [72,73] invokes following constraint on the ratio of $M_{Z_{BL}}$ and g_{BL} :

$$\frac{M_{Z_{BL}}}{g_{BL}} \geq 7 \text{ TeV}. \tag{21}$$

The corresponding bounds from the large hadron collider (LHC) experiment have become stronger than this by now as both the ATLAS and the CMS collaborations have performed dedicated searches for dilepton resonances in proton-proton collisions. The latest bounds from the ATLAS experiment [74,75] and the CMS experiment [76] at the LHC rule out such gauge boson masses below 4–5 TeV from analysis of 13 TeV centre of mass energy data. However, such limits are derived by considering the corresponding gauge coupling g_{BL} to be similar to the ones in electroweak theory and hence the bounds become less stringent for weaker gauge couplings [74]. Additionally, if such Abelian gauge bosons couple only to the third generation leptons, then the collider bounds get even weaker, as explored recently in a singlet–doublet fermion DM scenario by the authors of [77].

Additionally, the singlet scalar of the model is also constrained [78,79] as it can mix with the SM Higgs and hence can couple to SM fields. The strongest bound on such mixing in scalar singlet extension of the SM arises from W boson mass correction [80] at NLO. For singlet scalar mass 250 GeV $\lesssim M_{H_2} \lesssim$ 850 GeV, the singlet-SM Higgs mixing is constrained to be $0.2 \lesssim \sin\theta \lesssim 0.3$. For heavier singlet scalar masses $M_{H_2} > 850$ GeV, the bounds from the requirement of perturbativity and unitarity of the theory turn dominant which gives $\sin\theta \lesssim 0.2$. On the other hand, for lighter singlet scalar masses $M_{s_i} < 250$ GeV, the LHC and LEP direct search [81,82] and Higgs signal strength measurement [82] constrain the mixing angle as $\sin\theta \lesssim 0.25$. If the singlet scalar is even lighter say, lighter than SM Higgs mass $M_{H_2} < M_{H_1}/2$, SM Higgs can decay into a pair of singlet scalars. Latest measurements by the ATLAS collaboration restrict such SM Higgs decay branching ratio into invisible particles to be below 13% [83] at 95% CL.

4 Inflation

In this section, we describe the dynamics of inflation in detail and its predictions in view of the present experimental bounds. We identify the real part of singlet scalar field Φ as the inflation. Along with the renormalisable potential in Eq. (5), we also assume that Φ is non-minimally coupled to gravity. For earlier studies in this context, please see [84,85] and references therein. Related studies in supersymmetric gauged $B-L$ model can be found in [86]. For works guided by the same unifying principle of inflation, dark matter and neutrino mass, one may look at [87–90] as well as references therein.

We denote the inflation field as ϕ hereafter, which is same as the notation used for real part of Φ field in earlier sections. Thus the potential responsible for inflation is given by

$$V_{\text{Inf}}(\phi) = \frac{\lambda_2}{4}\phi^4 + \frac{\xi}{2}\phi^2 R, \tag{22}$$

where R stands for the Ricci scalar and ξ is a dimensionless coupling of singlet scalar to gravity. We have neglected the contribution of v_{BL} in Eq. (22) by considering it to be much lower than the reduced Planck mass M_P. The action for ϕ in Jordan frame takes the following form (apart from the couplings to the fermions and SM Higgs)

$$S_J = \int d^4x\sqrt{-g}\Big[-\frac{M_P^2}{2}\Omega(\phi)^2 R + \frac{1}{2}(D_\mu\phi)^\dagger(D^\mu\phi) - \frac{\lambda_2}{4}\phi^4\Big], \tag{23}$$

where $\Omega(\phi)^2 = 1 + \frac{\xi\phi^2}{M_P^2}$, g is the spacetime metric in the $(-,+,+,+)$ convention, $D_\mu\phi$ stands for the covariant derivative of ϕ containing couplings with the gauge bosons which just reduces to the normal derivative $D_\mu \to \partial_\mu$ (since during inflation, there are no fields other than the inflation).

In order to simplify the calculations, we make the following conformal transformation to write the action S_J in the Einstein frame [91,92]:

$$\hat{g}_{\mu\nu} = \Omega^2 g_{\mu\nu},\ \ \sqrt{-\hat{g}} = \Omega^4\sqrt{-g}, \tag{24}$$

so that it looks like a regular field theory action with no explicit couplings to gravity. In the above transformation, $\hat{g}$ represents the metric in the Einstein frame. To make the kinetic term of the inflation canonical, we redefine ϕ by

$$\frac{d\chi}{d\phi} = \sqrt{\frac{\Omega^2 + \frac{6\xi^2\phi^2}{M_P^2}}{\Omega^4}} = Z(\phi), \tag{25}$$

where χ is the canonical field. Using these inputs, the inflationary potential in the Einstein frame can be written as,

$$V_E(\phi(\chi)) = \frac{V_J\big(\phi(\chi)\big)}{\big(\Omega\big(\phi(\chi)\big)\big)^4} = \frac{1}{4}\frac{\lambda_2\phi^4}{\big(1+\frac{\xi\phi^2}{M_P^2}\big)^2}, \tag{26}$$

where $V_J(\phi)$ is identical to $V_{\rm Inf}(\phi)$ in Eq. (22). We then make another redefinition: $\Phi = \frac{\phi}{\sqrt{1+\frac{\xi\phi^2}{M_P^2}}}$ and reach at a much simpler from of V_E given by

$$V_E(\Phi) = \frac{1}{4}\lambda_2\Phi^4. \tag{27}$$

Note that for an accurate analysis, one should work with renormalisation group (RG) improved potential and in that case, λ_2 in Eq. (27) will be function of Φ such that,

$$V_E(\Phi) = \frac{1}{4}\lambda_2(\Phi)\Phi^4 \tag{28}$$

The one loop renormalisation group evolution (RGE) equations of the relevant parameters associated with the inflationary dynamics are given by,

$$\begin{aligned}\beta_{\lambda_2} &= (18s^2+2)\lambda_2^2 + 2\lambda_3^2 - \Big(48g_{BL}^2 - 2\Sigma_N^2\Big)\lambda_2 \\ &\quad + 96g_{BL}^4 - \Sigma_N^4,, \end{aligned} \tag{29}$$

$$\beta_\xi = \Big(\xi+\frac{1}{6}\Big)\Big((1+s^2\lambda_2) - 2\zeta\Big) \tag{30}$$

$$\beta_{g_{BL}} = \left(\frac{32+4s}{3}\right) g_{BL}^3 \tag{31}$$

$$\beta_{Y_{N_i}} = Y_{N_i}^3 - 6g_{BL}^2 Y_{N_i} + \frac{1}{2}Y_{N_i}\Sigma_N^2, \tag{32}$$

where we define $s = \left(1+\frac{\xi\phi^2}{M_P^2}\right)\left(1+(1+6\xi)\frac{\xi\phi^2}{M_P^2}\right)^{-1}$, $\zeta = \frac{1}{(4\pi)^2}\Big(\frac{1}{2}\Sigma_N^2 - 12g_{BL}^2\Big)$, $\Sigma_N^2 = \sum_{i=1}^3 Y_{N_i}^2$ and $\Sigma_N^4 = \sum_{i=1}^3 Y_{N_i}^4$ and $\beta_{x_i} = \frac{1}{16\pi^2}\frac{dx_i}{d\,\ln\Phi}$. The RGE equations for rest of the couplings are provided in Appendix A.

We choose the heavy neutrino mass spectrum, satisfying the hierarchy $M_{N_1} \ll M_{N_2} < M_{N_3}$ and a diagonal RH neutrino mass matrix. Note that, from this section onwards, we are denoting the RHNs as N_i only without denoting the chirality explicitly. For simplicity, we denote $Y_{N_{22}} \equiv Y_{N_2}, Y_{N_{33}} \equiv Y_{N_3}$. Thus the right handed neutrino mass hierarchy implies $Y_{N_1} \ll Y_{N_2} < Y_{N_3}$. Let us first analyse the case where the RG running of λ_2 is dominated by g_{BL} and $Y_{N_{2,3}}$. Then Eq. (29) can be rewritten as,

$$\beta_{\lambda_2} \simeq 96g_{BL}^4 - Y_{N_2}^4 - Y_{N_3}^4 + 2\lambda_3^2. \tag{33}$$

We ignore the contributions of λ_2 and Y_{N_1} in the R.H.S. of Eq. (33) considering them to be negligible.[3] Since λ_2 is very small, $\beta_{\lambda_2} \ll 0$ or $\beta_{\lambda_2} \gg 0$ can cause sharp changes in λ_2 value from its initial magnitude during the evolution. It may also happen that λ_2 becomes negative at some energy scale. Then the inflationary potential would turn unstable along ϕ field direction. Therefore the most acceptable case is to make $\beta_{\lambda_2} \to 0$ at least during inflation so that the inflationary potential remains stable [85]. To ensure $\beta_{\lambda_2} \simeq 0$, the equality $\Delta = 96g_{BL}^4 - 82Y_{N_2}^4 + 2\lambda_3^2 \sim 0$ has to be maintained, where we have assumed $Y_{N_3} = 3Y_{N_2}$. We can further simplify the expression for Δ by assuming $\lambda_3^2 \ll g_{BL}^4$. In Fig. 1, we show the RG running of λ_2 as a function of Φ for different values of g_{BL} considering (left panel) $\xi = 1$ and (right panel) $\xi = 0.1$. The λ_2 running for $\Delta \sim 0$ is shown in blue colour while the other colours represent the cases where the $\Delta \sim 0$ condition gets violated by $\pm 10\%$. Figure 1 clearly points out that indeed a small violation of the $\Delta \sim 0$ criteria can cause sharp instability of the inflationary potential.

In upper left panel of Fig. 2, we show the behaviour of the inflationary potential V_E as a function of Φ for different values of g_{BL} considering $\xi = 0.1$. The value of Σ_N^4 is determined from the equality Δ earlier defined. As it can be observed, with the increase of g_{BL}, the potential starts to develop a local minimum near some Φ value say, Φ_I. If such a local minimum exists, then the field could be trapped there and the inflation will stop rolling. This provides an upper bound on g_{BL} such that the local minimum of $V_E(\Phi)$ does not appear. The existence of a local minimum can be further confirmed if $\frac{dV_E(\Phi)}{d\Phi} \simeq 0$ near Φ_I. This condition can be rewritten as

$$\frac{dV_E}{d\Phi} = \frac{\beta_{\lambda_2}}{4} + \lambda_2(\Phi) \simeq 0. \tag{34}$$

We plot $\frac{dV_E}{d\Phi} = V_E'(\Phi)$ in upper right panel of Fig. 2 as a function of Φ. We observe that for $g_{BL} \gtrsim g_{BL}^{\rm max} = 0.045$, the inflationary potential indeed develops a local minimum near $\Phi_I = 4M_P$. Similar conclusion can be drawn for $\xi = 1$ as shown in lower panel of Fig. 2 . One important point to be noted is that the value of $g_{BL}^{\rm max}$ gets enhanced with the increase of ξ. We illustrate this in Fig. 3 where $g_{BL}^{\rm max}$ is plotted against different values of ξ.

[3] Unless the non-minimal coupling ξ is very large, the self-quartic coupling of inflation must be very small in order to be in agreement with correct inflationary parameters [93].

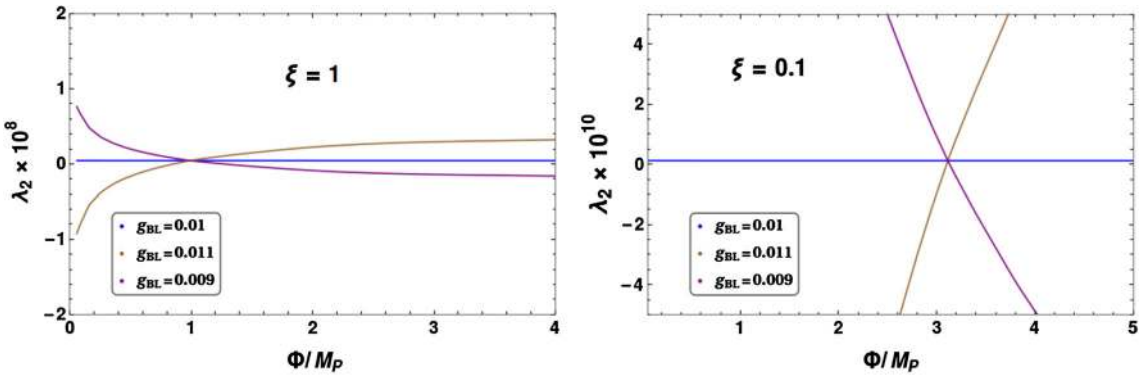

Fig. 1 RG running of λ_2 as function of Φ considering the stability condition (blue) $\Delta \sim 0$ with $\xi = 1$ (left panel) and $\xi = 0.1$ (right panel). Brown and purple curves show $\pm 10\%$ variation from $\Delta \sim 0$

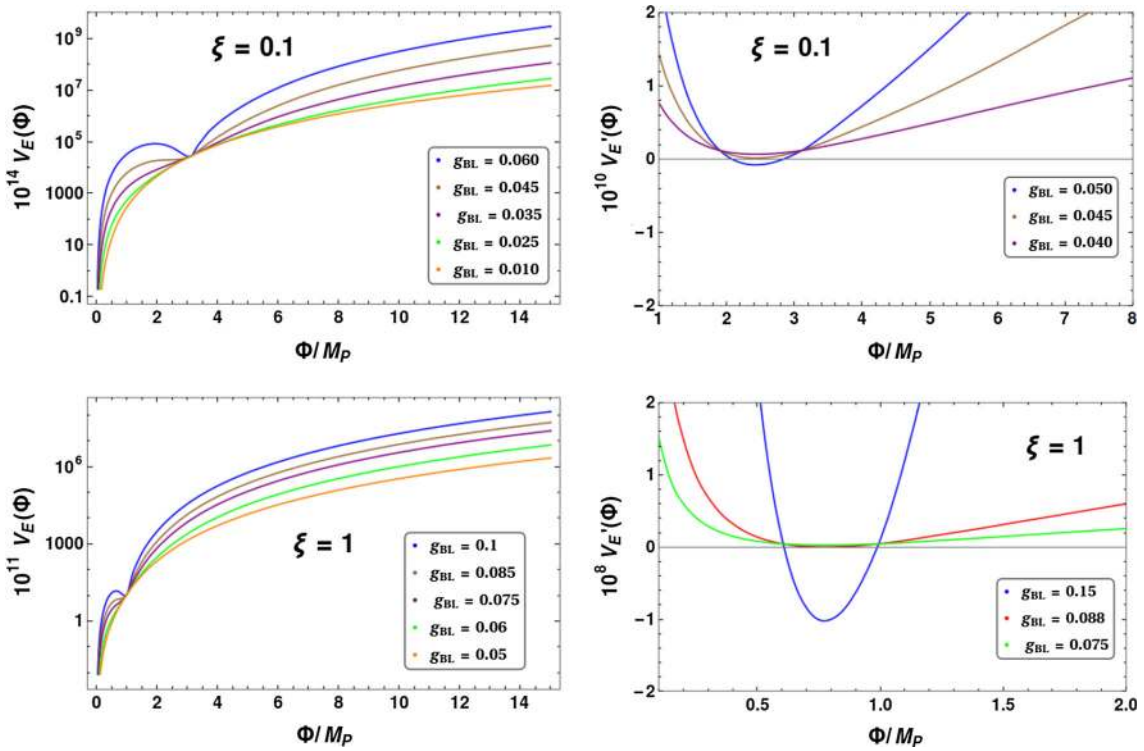

Fig. 2 (Left) The inflationary potential and (right) first derivative of the inflationary potential are plotted for different values of g_{BL} considering $\Delta \sim 0$ with $\xi = 0.1$ (top) and $\xi = 1$ (bottom)

Next, we move on to calculate the predictions for inflationary observables. In terms of the original field ϕ, the slow roll parameters (ϵ, η) and number of e-folds (N_e) are found to be

$$\epsilon(\phi) = \frac{M_P^2}{2Z(\phi)^2}\left(\frac{V_E'(\phi)}{V_E(\phi)}\right)^2, \tag{35}$$

$$\eta(\phi) = \frac{M_P^2}{Z(\phi)^2}\left(\frac{V_E''(\phi)}{V_E(\phi)} - \frac{V_E'(\phi)Z'(\phi)}{V_E(\phi)Z(\phi)}\right), \tag{36}$$

$$N_e = \int_{\phi_t}^{\phi_{end}} \frac{Z^2 V_E(\phi)}{V_E'(\phi)}\frac{d\phi}{M_{\rm P}}, \tag{37}$$

respectively. The inflationary observables such as spectral index (n_s), tensor to scalar ratio (r) and scalar perturbation spectrum (P_S) can be expressed in terms of the slow roll parameters as

$$n_s = 1 - 6\epsilon + 2\eta, \quad r = 16\epsilon, \quad P_S = \frac{V_E(\phi)}{24M_P^4\pi^2\epsilon}. \tag{38}$$

All these quantities have to be determined at the horizon exit of the inflation (ϕ_t) and we consider the number of e-folds $N_e = 60$ for the numerical analysis. We perform a numerical scan over g_{BL} and ξ to estimate the inflationary observables

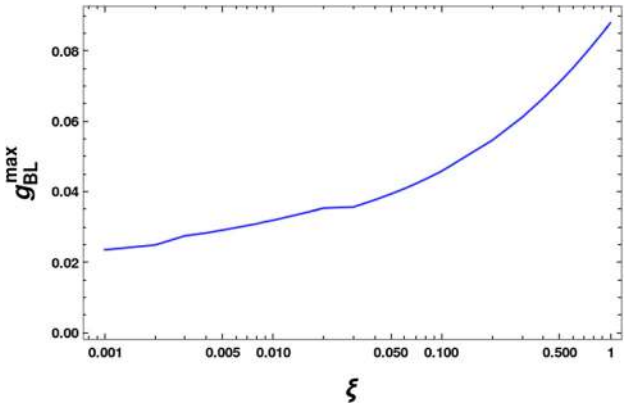

Fig. 3 Variation of $g_{BL}^{\max}$ as a function of ξ

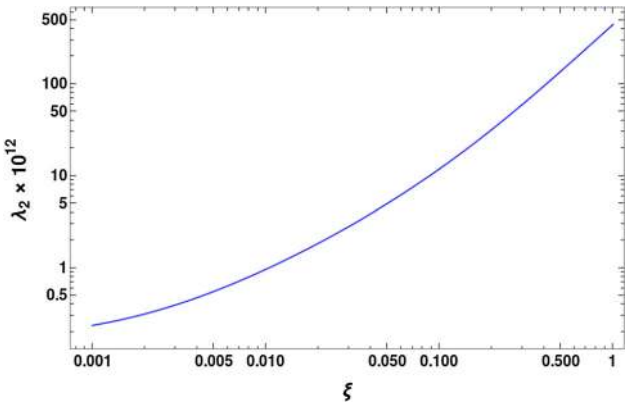

Fig. 4 Variation of λ_2 as a function ξ in order to produce the correct amount of curvature perturbation spectrum P_s

n_s and r considering $\Delta \sim 0$. The initial value of λ_2 is determined to produce the correct observed value of scalar perturbation spectrum P_S at horizon exit. In Fig. 4 we show the variation of λ_2 with ξ to be consistent with the observed value of $P_S = 2.4 \times 10^{-9}$. It turns out that the value of r does not change much with the variation of g_{BL} for a constant value of ξ since $\beta_\lambda = 0$ at inflationary energy scale. Contrary to this, value of n_s is quite sensitive to g_{BL}. We see from left panel of Fig. 5 that n_s increases with the enhancement of g_{BL} for different values of ξ. The rate of increase of n_s with g_{BL} turns flatter with the rise of ξ value. In the right panel of Fig. 5 we plot $n_s - r$ contours for different g_{BL} values and by varying ξ in the range 0.001–1. For comparison purpose we also insert the Planck 2018+BAO+BK15 1σ and 2σ bounds [2]. It is evident that the present setup is able to provide set of $n_s - r$ values, consistent with the experimental constraints. Finally, in the left panel Fig. 6, we constrain the $\xi - g_{BL}$ plane which correctly produces the $n_s - r$ values consistent with Planck 1σ (red) and 2σ (brown) bounds.

So far we have discussed the case where $g_{BL}^4, \Sigma_N^4 \gg \lambda_2^2$ at inflationary energy scale. Hence, it is obvious to consider the opposite limit of these parameters. When $g_{BL}^4, \Sigma_N^4 \ll \lambda_2^2$, automatically the inflation scenario merges with the case of quartic inflation and non minimal coupling of inflation to gravity as originally studied in [93]. For completeness purpose we discuss this particular case in right panel of Fig. 6 in $n_s - r$ plane. As it is seen the $n_s - r$ contour can still satisfy the Planck 2018 1σ bounds for $N_e = 60$. The contour of observed value of P_S in $\xi - \lambda_2$ plane remains same as in Fig. 4.

4.1 Reheating

Once inflation ends, the thermalisation of the universe, leading to a radiation dominated universe has to be ensured. This is the reheating epoch [94], which takes the universe from the inflationary phase to the radiation-domination phase.

Originally, the reheating process was proposed as the perturbative decay of inflation field into lighter degrees of freedoms [95]. During oscillation, the energy of inflation gets transferred into the relativistic lighter decay products. Approximately, the amount of energy density of the radiation bath is obtained as $\sim 3M_P^2\Gamma_\Phi$ where Γ_Φ is the total decay width of inflation. Considering inflation decay into radiation only while setting up thermodynamic equilibrium quickly after the decay, the maximum reheating temperature of the universe is found to be

$$T_R \sim \left(\frac{90}{g_*\pi^2}\right)^{1/4} \sqrt{\Gamma_\Phi M_P}, \tag{39}$$

where g_* is the number of relativistic degrees of freedom in the thermal bath.

However, the success of this perturbative decay mechanism of inflation is somewhat limited. In initial stages of reheating, the phenomena of parametric resonance might be important and may lead to explosive particle production which the theory of perturbative reheating does not take into account. This dynamics is known as preheating [96–98]. In particular, if the oscillation amplitude of the inflation is sufficiently large, the number density of the produced bosonic particles might be enhanced ($n_k \gg 1$) due to the effects related to Bose statistics. In an expanding universe, this process occurs in a stochastic manner, and is known as stochastic resonance. The produced particles, due to the large amplitude of inflation, turn non-relativistic and further decay into lighter relativistic particles. The primary condition which needs to be satisfied to attain parametric resonance in an inflationary framework is that the decay width of non-relativistic particles should be less than its production rate. Parametric resonance halts once the inflation oscillation amplitude becomes small and the resonance becomes narrower.

The presence of parametric resonance as described above could raise the final reheating temperature compared to the one obtained by considering the perturbative reheating only.

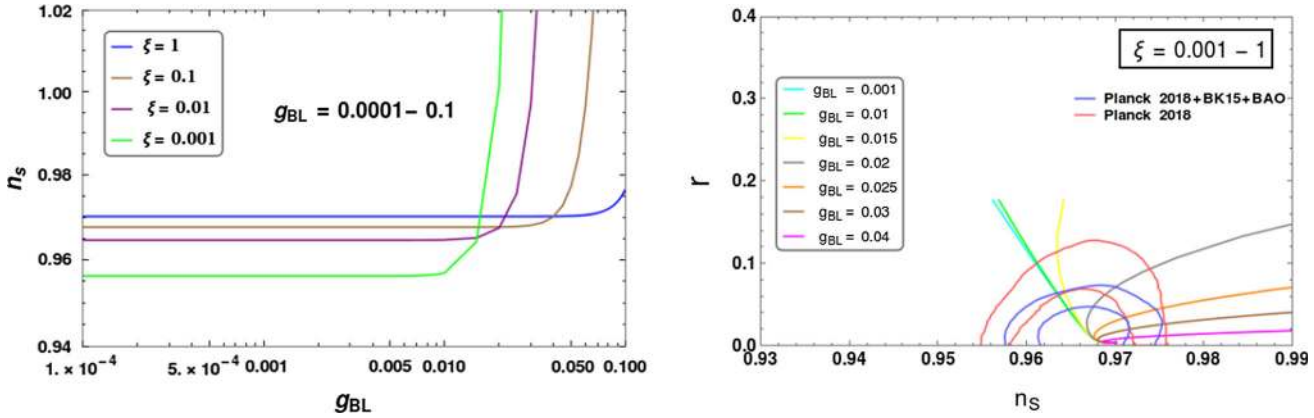

Fig. 5 (Left) The magnitude of spectral index n_s is plotted against g_{BL} for different ξs. (Right) $n_s - r$ contours for different set of constant g_{BL} values with $\xi = 0.001 - 1$. The 1σ and 2σ bounds from Planck 2018+BAO+BK15 are also included

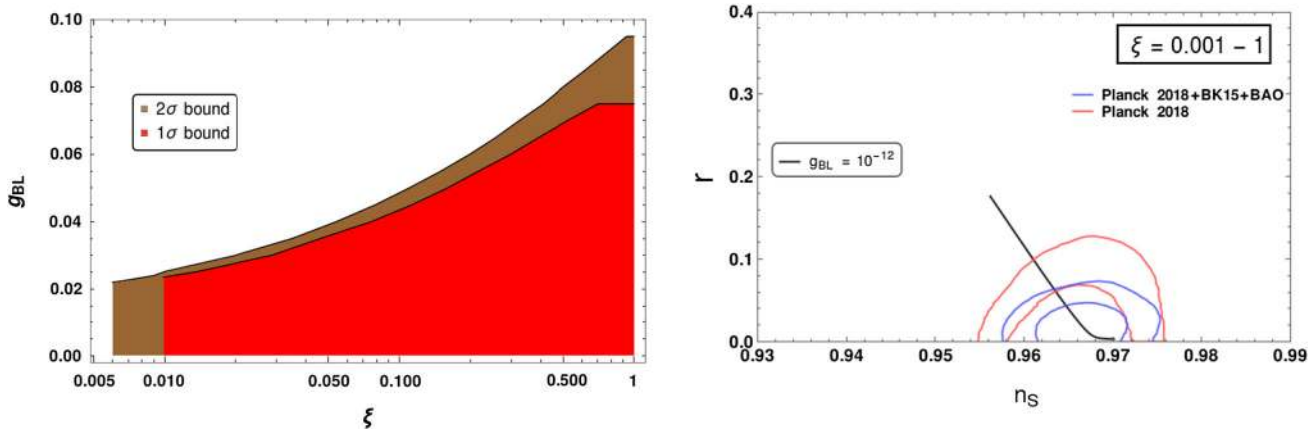

Fig. 6 (Left) Allowed parameter space from inflation in $g_{BL} - \xi$ plane by Planck 2018 1σ and 2σ bounds. (Right) $n_s - r$ contour by varying ξ and considering g_{BL}^4, $\Sigma_N^4 \ll \lambda_2^2$ at inflationary energy scale for $N_e = 60$

However, if the couplings of the inflation with the lighter particles are not strong enough, the resonance is narrow or not broad enough. This makes preheating inefficient. In particular, it was shown in Refs. [97,98] that for couplings $\lesssim \mathcal{O}(10^{-4})$ the broad resonance does not take place (resulting $n_k \ll 1$ [98,99]) and preheating finishes at very early stage without posing significant impact on the final reheating temperature. In that case the reheating temperature of the universe is dominantly guided by the perturbative reheating.

From the inflationary perspective, we are having two different kind of scenarios having phenomenological relevance namely, (i) g_{BL}^4, $\Sigma_N^4 \gg \lambda_2^2$ and (ii) g_{BL}^4, $\Sigma_N^4 \ll \lambda_2^2$.

For the first case g_{BL} is large and thus $\Delta \sim 0$ is an essential condition for the stability of inflationary potential. We consider $\lambda_3 \ll g_{BL}^2$ so that it does not effect the evolution of Δ significantly. This assumption was made earlier also while determining the fate of inflation. The value of Δ as defined earlier changes by small amount in its RG evolution (see right panel of Fig. 7). It is found that the value of $\lambda_2(\Phi_I)$ changes by order of magnitudes at low scale, for example $\lambda_2(\Phi = 1\,\text{TeV})$ becomes $\mathcal{O}(10^{-6})$ from 4.34×10^{-10} at inflationary scale (considering $\xi = 1$, see left panel of Fig. 7). During preheating stage, first Z_{BL}, SM bosons get produced during the oscillation regime. Afterwards due to inflation induced large mass these produced Z_{BL} and SM bosons turn non-relativistic, and they decay into the lighter relativistic particles. In a whole, this particular process comprises of unusual stochastic resonance production of lighter non relativistic particles, their further decays, backreaction in the presence of an expanding universe. Hence the estimate of the correct reheating temperature is more involved and requires rigorous lattice simulation [100,101]. Since we shall see in a while that this scenario turns out to be disfavoured due to overproduction of WIMP DM relic, we do not elaborate on this further.[4]

In the second case g_{BL}^4, $\Sigma_N^4 \ll \lambda_2^2$, the inflationary potential is mainly driven by λ_2 with other couplings sufficiently

[4] In Refs. [90,102] a detailed analysis on preheating in a similar setup has been performed considering $\xi \gg 1$.

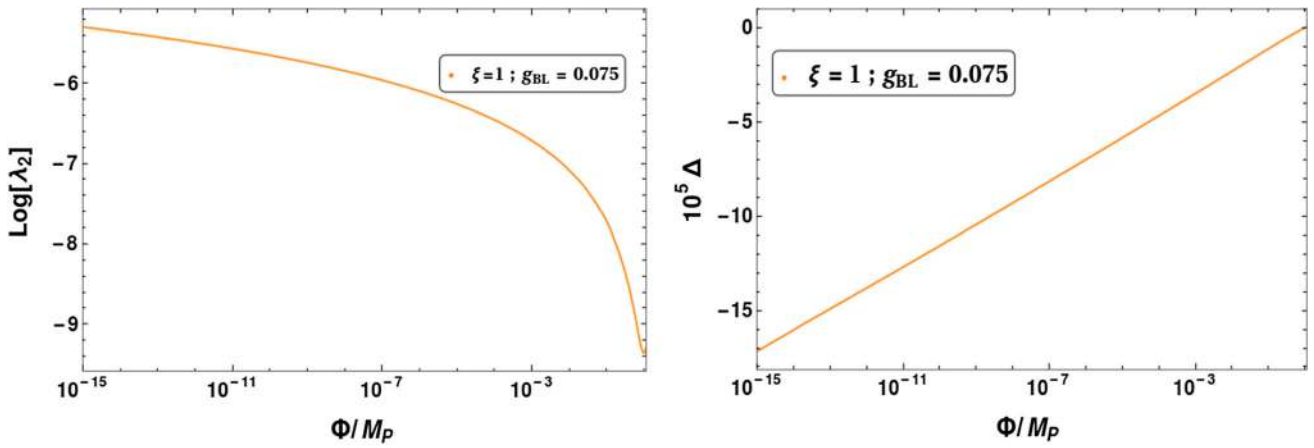

Fig. 7 RG running of λ_2 (left) and Δ (right) as function of the energy scale Φ considering $\xi = 1$ and $g_{BL} = 0.075$

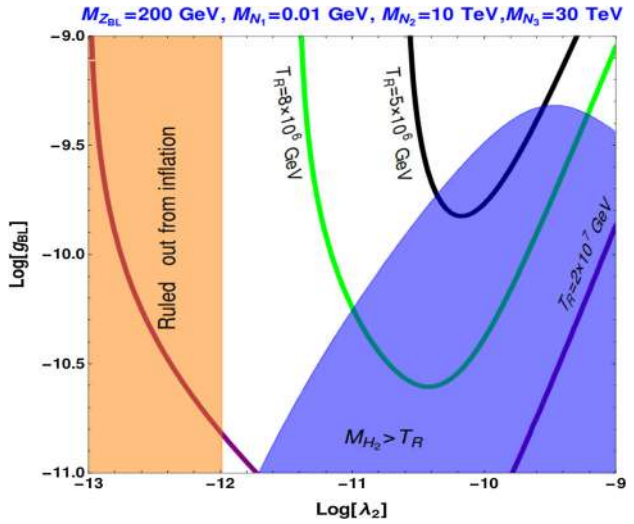

Fig. 8 Case II: Contours of T_R in $g_{BL} - \lambda_2$ plane considering fixed values of $M_{Z_{BL}}$, $M_{N_{1,2,3}}$. The orange region is ruled out from inflation and in the blue region mass of the inflation is larger than the reheating temperature

small. Hence $\Delta \sim 0$ is not a necessary condition for this case. However the coupling λ_3 (we take $\mathcal{O}(10^{-10})$) should be still much smaller than unity so that the stability of inflation potential remains intact. Here, due to the smallness of all relevant couplings there will not be any significant changes during their RG running unlike in the earlier case. The important point is with the estimates of g_{BL} and λ_3 from inflation, the preheating stage never turns efficient and gets over at very early stage of inflation oscillation. Then the reheating of the universe will be effectively dictated by the perturbative decay of inflation. Here, depending on the mass scale (or λ_2), the tree level decay of inflation into $Z_{BL}Z_{BL}$, $H_1 H_1$ final states are possible. The inflation can also decay into right handed neutrinos, if kinematically allowed. In Fig. 8 we show the contours of different values of T_R (ranging from 5×10^6 GeV $- 2 \times 10^7$ GeV) in $g_{BL} - \lambda_2$ plane. For this purpose we fix $M_{Z_{BL}} = 200$ GeV, $M_{N_1} = 10$ MeV, $M_{N_2} = 10$ TeV and $M_{N_3} = 30$ TeV. The orange coloured region is ruled out from the requirement of reproducing the observed value of scalar perturbation spectrum P_S at horizon exit. In the blue coloured region inflation mass turns larger than the reheating temperature and hence it remains out of equilibrium. This may have important implications for other related phenomenology as we will discuss in a while.

5 Dark matter

In this section, we discuss the dark matter phenomenology in detail and attempt to find its consistency with the inflationary dynamics. As mentioned earlier, N_1 is the DM candidate which is odd under Z_2 and hence stable. For earlier studies of DM in this model, one may refer to [104–108]. While the Z_2 odd RHN is the DM candidate, the other two RHN's take part in the usual type I seesaw mechanism, giving rise to light neutrino masses and mixing. Since DM is a singlet under SM gauge symmetry, it can interact with the visible sector particles only via gauge (Z_{BL}) or scalar (H_2) interactions. Now, depending upon the two cases namely, (i) $g_{BL}^4, \Sigma_N^4 \gg \lambda_2^2$ and (ii) $g_{BL}^4, \Sigma_N^4 \ll \lambda_2^2$ discussed in the context of inflation, DM-SM couplings can either be of order unity or very small. This will lead to completely different DM phenomenology namely, thermal or WIMP type and non-thermal or FIMP type, which we discuss separately below.

For the first case, that is, $g_{BL}^4, \Sigma_N^4 \gg \lambda_2^2$, it is expected that the DM stays in thermal equilibrium with the SM particles in the early universe and thus falls into the WIMP category. The DM can annihilate into different final states in the thermal bath through processes mediated by scalars and the $U(1)_{B-L}$ gauge boson. In Fig. 9, we exhibit the possible annihilation processes of N_1 in the present framework. Please note that,

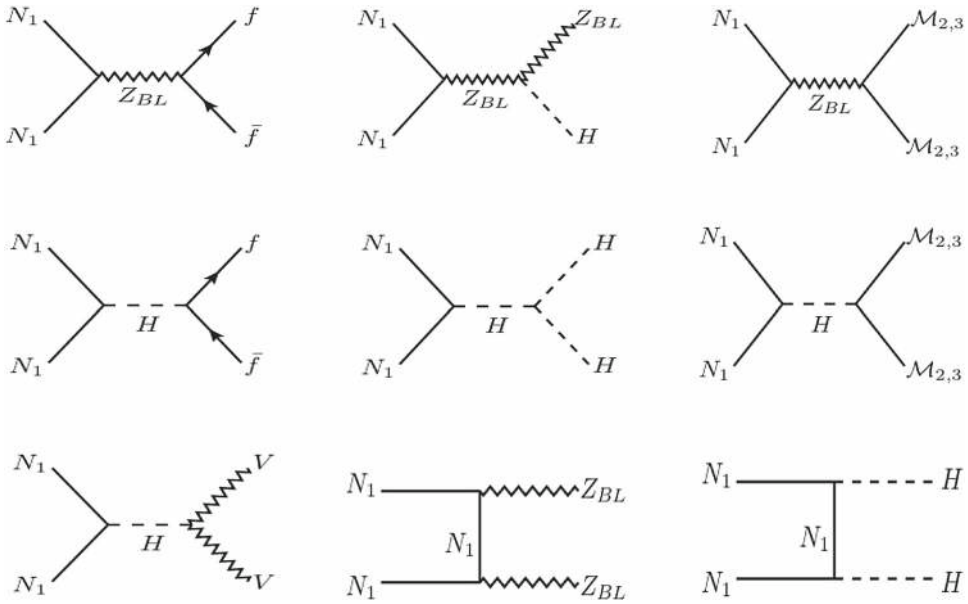

Fig. 9 All possible annihilation processes of DM (N_1) into various final state particles. Here, $\mathcal{M}_{2,3}$, H and V represent the Majorana neutrinos ($N_{2,3}$ or $\nu_{2,3}$), scalars H_1, H_2 and electroweak vector bosons respectively

in principle, the symmetry of the model allows a kinetic mixing term between $U(1)_Y$ of SM and $U(1)_{B-L}$ of the form $\frac{\varepsilon}{2}B^{\alpha\beta}B'_{\alpha\beta}$ where $B^{\alpha\beta} = \partial^\alpha B^\beta - \partial^\beta B^\alpha$ and ε is the mixing parameter. Even if we turn off such mixing at tree level as we have done here, one can generate such mixing at one loop level since there are particles in the model which are charged under both $U(1)_Y$ and $U(1)_{B-L}$. Such one loop mixing can be approximated as $\varepsilon \approx g_{\rm BL}g_2/(16\pi^2)$ [109]. Since $g_{\rm BL}$ has tight upper bound from inflationary dynamics, the one loop mixing can be neglected in comparison to other relevant couplings and processes. Therefore, for simplicity, we ignore such kinetic mixing for the rest of our analysis.

5.1 WIMP DM scenario

The evolution of comoving number density of DM ($Y_{\rm DM} = n_{\rm DM}/s$) is determined by the corresponding Boltzmann equation

$$\frac{dY_{\rm DM}}{dz} = -\frac{z\langle\sigma v\rangle s}{\mathcal{H}(M_{N_1})}\left(Y_{\rm DM}^2 - Y_{\rm DM}^{\rm eq^2}\right), \tag{40}$$

where

$$Y_{\rm DM}^{\rm eq^2} = \frac{45}{4\pi^4}\frac{g}{g_{*s}}z^2K_2(z), \tag{41}$$

with g and g_{*s} being the internal degrees of freedom of the dark matter and relativistic entropy degrees of freedom respectively and $z = M_{N_1}/T$. The $\langle\sigma v\rangle$ in Eq. (40) stands for the thermally averaged cross section of DM annihilation, given by [110]

$$\langle\sigma v\rangle = \frac{1}{8M_{N_1}^4TK_2^2\left(\frac{M_{N_1}}{T}\right)}\int_{4M_{N_1}^2}^{\infty}\sigma(s-4M_{N_1}^2)\sqrt{s}\,K_1\left(\frac{\sqrt{s}}{T}\right)ds, \tag{42}$$

where $K_i(z)$'s are modified Bessel functions of order i. $\mathcal{H}(M_{N_1})$ represents the Hubble parameter at $T = M_{N_1}$.

We implement the model in `FeynRules` [111] and then use `micrOMEGAs` package [112] to estimate the relic abundance of DM numerically. The independent parameters which participate in determining the DM relic abundance are the following:

$$\left\{Y_{N_{2,3}}, Y_{D_{ij}}, M_{Z_{BL}}, g_{BL}, M_{H_2}, M_{N_1}, \sin\theta\right\}. \tag{43}$$

In our case, we have considered the Y_N matrix diagonal and the sum of fourth power of each diagonal elements are fixed by inflationary requirements. However, for the DM analysis we need the magnitude of each individual elements. For simplification purpose we make the choice $Y_{N_3} = 3Y_{N_2}$ at the inflationary energy scale, to reduce the number of free parameters. The $\Delta \sim 0$ condition was essential at the inflationary energy scale and hence for the DM analysis we need to run the RGE equations of g_{BL} and Y_N along with λ_2 and λ_3, with the initial condition $\Delta = 0$, to estimate their values around few TeV scale, relevant for DM freeze-out. The value of Y_{N_1} will be fixed from the choice of DM mass and then the magnitude of $M_{N_{2,3}}$'s can be computed using $Y_{N_{2,3}}$ values obtained at TeV scale through RG running. Since Y_{N_1} is taken to be smaller than $Y_{N_{2,3}}$, DM mass M_{N_1} is smaller than $M_{N_{2,3}}$'s. We have already discussed the Dirac neutrino Yukawa or Y_D matrix and here we use the same form as defined in Eq. (19) using Casas–Ibarra parametrisation. Here we work with $\lambda_2 = 4.35 \times 10^{-10}$ (corresponding to $\xi = 1$, see Fig. 4), $\lambda_3 = 10^{-6}$ at inflationary energy scale. Since in our working range of gauge coupling $0.01 < g_{BL} < 0.075$, the reheating temperature T_R is expected to be large, hence it is obvious that the relevant SM and BSM fields will maintain thermal equilibrium with each other.

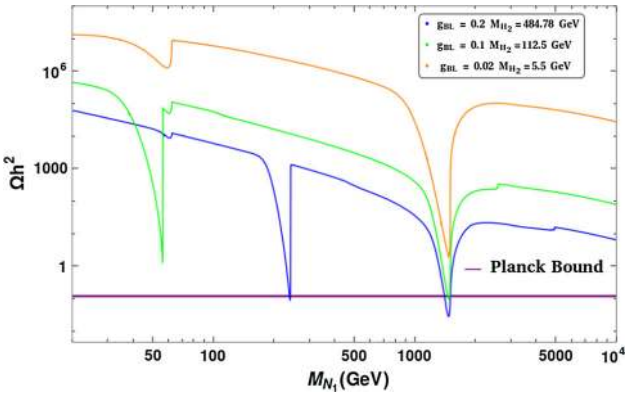

Fig. 10 DM Relic as a function of its mass for different set of g_{BL} values with $M_{Z_{BL}} = 3$ TeV. We have considered $\lambda_2 = 4.35 \times 10^{-10}$ and $\lambda_3 \sim 10^{-6}$ at inflationary energy scale

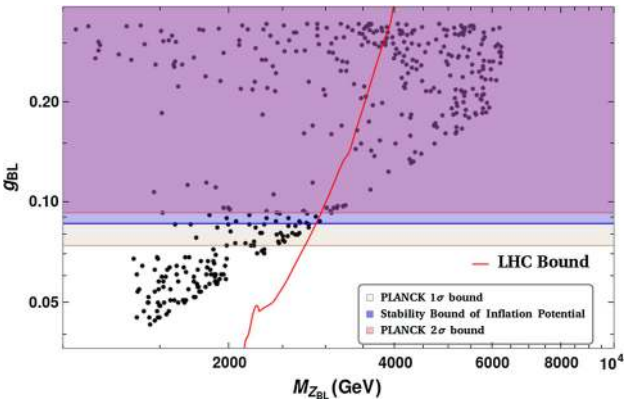

Fig. 11 Parameter space satisfying DM relic abundance in $g_{BL} - M_{Z_{BL}}$ plane by considering $\lambda_2 = 4.35 \times 10^{-10}$ and $\lambda_3 \sim 10^{-6}$ at inflationary energy scale. Bounds arising from LHC, Planck constraints on inflation (1σ and 2σ) and stability of inflationary potential are also shown. The shaded regions are disallowed

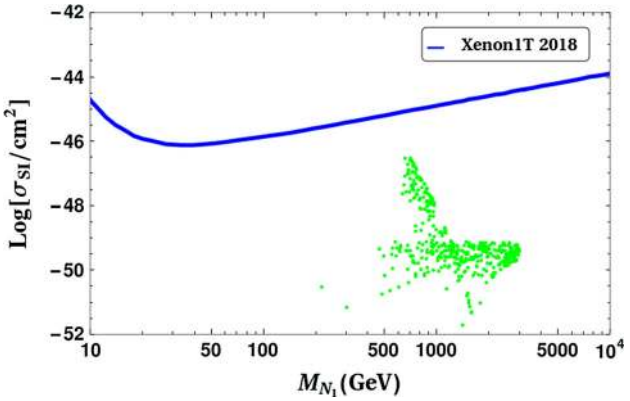

Fig. 12 Direct detection cross sections of the relic satisfied points (green dots) in Fig. 11 as function of DM mass is shown along with the bound from XENON1T [29,30]

In Fig. 10, we show the variation of relic as function of DM mass for different set of g_{BL} values (at inflationary energy scale) by keeping $M_{Z_{BL}}$ fixed at 3 TeV. The order of magnitude of λ_2 and λ_3 are determined at TeV scale through their RG running corresponding to different H_2 mass and $H_2 - H_1$ mixing. With the choices of different mass scales, three resonances appear for Ω lines at $\frac{M_{H_1}}{2}$, $\frac{M_{H_2}}{2}$ and $\frac{M_{Z_{BL}}}{2}$ respectively. In some cases, one of the scalar resonances is not so prominent due to smallness of H_2 mass or $H_2 - H_1$ mixing. The purple solid line in Fig. 10 represents the observed relic abundance, as per Planck 2018 data [3]. It is seen that the annihilation through gauge boson is the most efficient one and can satisfy correct relic in two out of three scenarios discussed.

We then perform a numerical scan to find the parameter space satisfying correct DM relic. In Fig. 11, we display the points satisfying correct DM relic (black dots) in $M_{Z_{BL}} - g_{BL}$ plane considering $M_{Z_{BL}} \lesssim 10$ TeV. We use the values of relevant parameters as earlier mentioned. We also include the LHC bound from dilepton resonance searches [74] (red curve), Planck constraints on inflation and stability bounds of the inflationary potential for comparison purpose. The shaded regions are disfavoured from the respective constraints. To conclude, we observe that with TeV scale or lower Z_{BL} mass, it is not possible to generate the correct value of relic abundance for WIMP dark matter while being in agreement with LHC and inflationary observables simultaneously. We also check that direct detection limits on spin-independent DM-nucleon cross section from the XENON1T experiment [29,30] and find that such bounds do not put any additional constraint on this parameter space as all the points shown in Fig. 12 obey these bounds.

5.2 FIMP DM scenario

In the second case (g_{BL}^4, $\Sigma_N^4 \ll \lambda_2^2$), the couplings responsible for DM-SM interactions are tiny and hence it is expected that DM may never reach thermal equilibrium with the standard bath. This falls under the ballpark of FIMP dark matter, discussed earlier. For earlier work on fermion singlet as FIMP DM in $U(1)_{B-L}$ model, please see [113,114] and references therein. A recent study also discussed the possibility of scalar singlet responsible for breaking $B-L$ gauge symmetry spontaneously to be a long-lived FIMP DM candidate [115]. If N_1 is a FIMP candidate, it can be produced non-thermally, due to decay or annihilation of other particles. In case Z_2 symmetry is exact, N_1 will be only pair produced as it is the only Z_2 odd particle. All scattering processes shown in Fig. 9 while discussing WIMP scenario can potentially contribute to the production of FIMP DM as well, when considered in the reverse direction. In addition, decays of $H_{1,2}$ and Z_{BL}, if kinematically allowed, can also contribute to the relic density of N_1. Typically, if same dimensionless couplings govern the strength of both decay and annihilation processes, the former

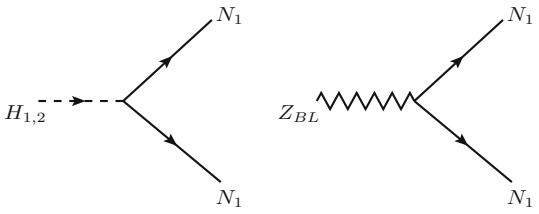

Fig. 13 DM production channels from tree level decay of heavier particles

dominates simply due to power counting. This is precisely the scenario here and FIMP is primarily produced from decays.

For our numerical calculation, we choose $\lambda_2 \sim 1.04 \times 10^{-12}$ at inflationary energy scale corresponding to $\xi \sim 0.01$ from inflationary requirements (see Fig. 4). Then from Fig. 8, it is evident that for this choice of λ_2, H_2 would be in thermal equilibrium with other SM particles by virtue of its coupling with Higgs as well as heavy right handed neutrinos $N_{2,3}$ which also maintain equilibrium since their masses considered here are below T_R and they can interact to SM fields through Yukawa interaction. We would like to keep $\lambda_3 \sim 10^{-10}$ extremely small so that it does not alter the RG running of λ_2 during inflation. Since g_{BL} is also very small to justify FIMP nature of DM, we will investigate the possibility of production of N_1 DM from non thermal tree level decays of Z_{BL} and H_2 (see Fig. 13). We will consider two benchmark choices of $M_{Z_{BL}} < 10$ TeV for the analysis. It is to be noted that Z_{BL} which interacts only via gauge coupling g_{BL} is also expected to be out of equilibrium. Hence non-thermal production of Z_{BL} from other bath particles and its subsequent decay into N_1 pairs play non-trivial roles. We therefore use coupled Boltzmann equations for both Z_{BL} and N_1 to calculate the relic abundance of N_1 in this scenario.

The evolution of the comoving number densities for Z_{BL} and DM are governed by the following coupled Boltzmann equations [113]

$$\frac{dY_{Z_{BL}}}{dz} = \frac{2M_P}{1.66M_{H_1}^2}\frac{z\sqrt{g_*(z)}}{g_{*s}(z)}\Big(\langle\Gamma_{H_{1,2}\to Z_{BL}Z_{BL}}\rangle\left(Y^{\rm eq}_{H_{1,2}} - Y_{Z_{BL}}\right) - \langle\Gamma_{Z_{BL}\to \rm all}\rangle Y_{Z_{BL}}\Big), \tag{44}$$

$$\begin{aligned}\frac{dY_{\rm DM}}{dz} &= \frac{2M_P}{1.66M_{H_1}^2}\frac{z\sqrt{g_*(z)}}{g_{*s}(z)}\Big(\langle\Gamma_{H_{1,2}\to N_1N_1}\rangle(Y^{\rm eq}_{H_{1,2}} - Y_{\rm DM}) \\ &\quad + \langle\Gamma_{Z_{BL}\to N_1N_1}\rangle(Y_{Z_{BL}} - Y_{\rm DM})\Big) \\ &\quad + \frac{4\pi^2}{45\times 1.66}\frac{g_{*s}}{\sqrt{g_*}}\frac{M_{H_1}M_P}{z^2} \\ &\quad \times\Big\{\langle\sigma v_{xx\to N_1N_1}\rangle\left(Y_x^{\rm eq^2} - Y_{\rm DM}^2\right) \\ &\quad + \langle\sigma v_{Z_{BL}Z_{BL}\to N_1N_1}\rangle(Y^2_{Z_{BL}} - Y^2_{\rm DM})\Big\},\end{aligned} \tag{45}$$

where $z = M_{H_1}/T$ and x represents all possible initial states. $g_*(z)$ is defined by

$$\sqrt{g_\star(z)} = \frac{g_{*s}(z)}{\sqrt{g_\rho(z)}}\left(1 - \frac{1}{3}\frac{{\rm d}\ln g_{*s}(z)}{{\rm d}\ln z}\right) \tag{46}$$

while g_{*s} is same as defined earlier. Here, $g_\rho(x)$ denotes the effective number of degrees of freedom related to the energy density of the universe at z. The $\langle\Gamma_{A\to BC}\rangle$ denotes the thermally averaged decay width which is given by

$$\langle\Gamma_{A\to BC}\rangle = \frac{K_1(z)}{K_2(z)}\Gamma_{A\to BC}. \tag{47}$$

Since initial densities of both Z_{BL} and N_1 are almost vanishing, one can ignore $Y_{Z_{BL}}$ and $Y_{\rm DM}$ from first term within each bracket on right hand side of Eqs. (44) and (45).

In left panel of Fig. 14, we show the evolution of $Y_{Z_{BL}}$ against z for benchmark choices of g_{BL} and other relevant parameters indicated in the figure. It is seen that $Y_{Z_{BL}}$ starts from a vanishingly small value initially and reaches a sizeable value with the lowering of temperature very quickly. The initial increase in Z_{BL} abundance happens primarily from H_2 decays. As expected, the production of Z_{BL} from H_2 decay becomes efficient around $T \sim M_{H_2}$ which corresponds to $z = M_{H_1}/T \sim 10^{-3}$. For $T < M_{H_2}$ there is a Boltzmann suppression in the equilibrium abundance of H_2 which makes Z_{BL} production less efficient leading to the plateau region where $Y_{Z_{BL}}$ remains more or less constant. We also observe that a larger value of g_{BL} while keeping $M_{Z_{BL}}$ fixed gives larger yield for Z_{BL}. The reason behind this is two-fold. Firstly, the partial decay width of H_2 into Z_{BL} pairs rises with the increase in g_{BL} values for our chosen benchmark points. Note that this partial decay width is function of g_{BL}, M_{H_2} and can be expressed as (in the limit $M^2_{Z_{BL}} \ll M^2_{H_2}, \theta \ll 1$)

$$\Gamma(H_2 \to Z_{BL}Z_{BL}) \approx \frac{g_{BL}^2 M_{H_2}^3}{8\pi M^2_{Z_{BL}}}. \tag{48}$$

Now, increase in g_{BL} corresponds to smaller M_{H_2} as evident by combining Eqs. (17) and (11) for a fixed $M_{Z_{BL}}$. Hence in general, enhancement of g_{BL} does not always mean higher value of $\Gamma(H_2 \to Z_{BL}Z_{BL})$. However numerically, we find that for the chosen benchmarks of Fig. 14, even though M_{H_2} decreases with increase in g_{BL}, the above decay width still increases by a factor of order one which enhances the yield of Z_{BL} by some amount. Secondly, a lighter H_2 will have comparatively lesser Boltzmann suppression in its equilibrium number density. These two factors, with the latter being dominant, lead to the enhancement of Z_{BL} (approximately by order of two), given other relevant parameters remain same. The production of Z_{BL} from H_1 decay will be mixing suppressed due to smallness of λ_3. It is in fact kinematically forbidden for the chosen benchmark values of Z_{BL} mass. For some epochs the abundance of Z_{BL} remains constant

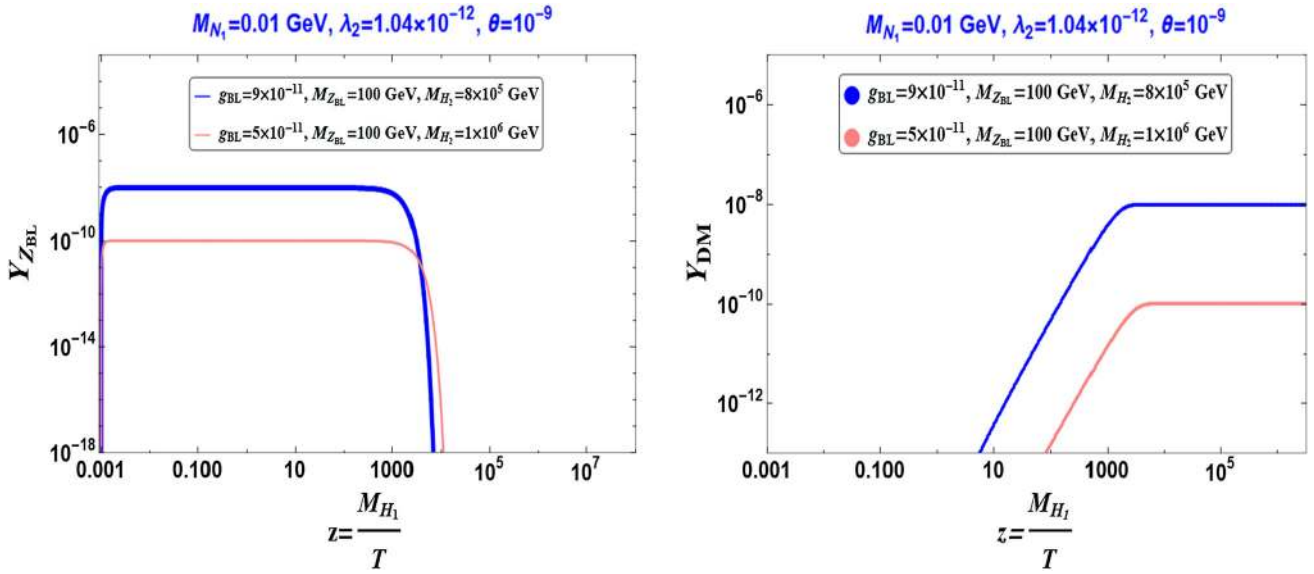

Fig. 14 Evolution of comoving number densities of Z_{BL} (left panel) and DM N_1 (right panel) as function of temperature

(denoted by the plateau region) and then gets reduced to zero again due to subsequent decays of Z_{BL} into N_1 as well as other lighter particles.

Similar features can be observed in right panel of Fig. 14 where the evolution of N_1 abundance is shown using the same choice of parameters as in left panel. The N_1 abundance begins from vanishingly small value and gets enhanced due to non-thermal production from Z_{BL} and H_2 decays and finally gets saturated. We notice that larger g_{BL} value leads to larger final abundance of the DM due to both the enhanced abundance of Z_{BL} (as earlier mentioned) as well as larger partial decay width of Z_{BL} into DM pairs. It is also relevant to mention here that in our working regime $M_{N_1} \ll M_{Z_{BL}}$, the associated Yukawa coupling (Y_{N_1}) with H_2 is suppressed compared to g_{BL} and hence direct production of DM is primarily dominated from tree level Z_{BL} decay.

Once the freeze-in abundance of DM that is $Y_{\rm DM}$ saturates, one can obtain the present relic abundance using the following expression:

$$\Omega_{\rm DM}h^2 = 2.755 \times 10^8 \left(\frac{M_{N_1}}{\rm GeV}\right) Y_{\rm DM}^{\rm present}. \tag{49}$$

Here $\Omega_{\rm DM} = \frac{\rho_{\rm DM}}{\rho_c}$, where $\rho_{\rm DM}$ is the DM energy density and $\rho_c = \frac{3\mathcal{H}_0^2}{8\pi G_N}$ is the critical energy density of the universe, with G_N being Newton's gravitational constant and $\mathcal{H}_0 \equiv 100\ h$ km s^{-1} Mpc^{-1} is the present-day Hubble expansion rate.

Using the above Eq. (49), we now find some benchmark parameters of our model which satisfy the correct DM abundance in the present universe. In Fig. 15, we have shown the DM yield evolutions for two set of parameters that

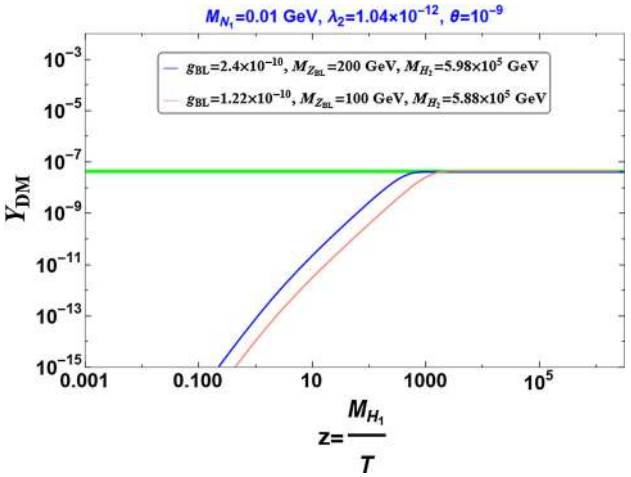

Fig. 15 Evolution of comoving number densities for the DM N_1 as function of temperature for two different sets of (g_{BL}, $M_{Z_{BL}}$) as tabulated in Table 3. Note that, the two set of reference points used here gives correct relic abundance (green region) in the present universe

matches with the observed relic bound (green shaded region) at $z \to \infty$. In Table 3 we list the numerical values of the parameters used in Fig. 15. As mentioned earlier, for such benchmark values of parameters the contribution of $2 \to 2$ scattering processes to DM production in the present analysis remains sub-dominant or negligible. It should be noted that while the required FIMP DM relic abundance can be successfully generated in this model, the corresponding parameter space leads to decoupling of $B - L$ gauge sector from inflationary dynamics leading to a usual quartic plus non-minimal inflation [93].

So far, the analysis on non thermal production of dark matter is performed by assuming H_2 in thermal equilibrium

Table 3 Two sets of parameters which can account for correct relic abundance for the FIMP case taking $\xi = 0.01$ from the inflationary dynamics, considering H_2 can be produced thermally ($M_{H_2} < T_R$)

g_{BL}	$M_{Z_{BL}}$	M_{H_2}	λ_2	Y_{N_1}	$Y_{N_2}(Y_{N_3})$	$\sin\theta$
2.4×10^{-10}	200 GeV	5.98×10^5 GeV	1.04×10^{-12}	1.7×10^{-14}	$10^{-6}(3 \times 10^{-6})$	10^{-9}
1.22×10^{-10}	100 GeV	5.88×10^5 GeV	1.04×10^{-12}	1.7×10^{-14}	$10^{-6}(3 \times 10^{-6})$	10^{-9}

with the SM bath. This is possible when $M_{H_2} < T_R$ and H_2 has sizeable couplings with other particles in the bath. However, it is also possible that M_{H_2} remains larger compared to the reheat temperature $M_{H_2} > T_R$ and hence the inflation remains out of equilibrium afterwards (see blue coloured region of Fig. 8). In such a case, the production of Z_{BL} and N_1 will not be possible like the way it was discussed before. Since SM Higgs mixing with H_2 is also very small, it is not possible to generate correct FIMP abundance. While interactions by virtue of gauge coupling and Yukawa coupling with H_2 are insufficient to produce correct FIMP abundance, one can turn to Yukawa couplings with ordinary leptons which are present in thermal bath for most of the epochs. However one has to get rid of the Z_2 symmetry in order to introduce such Yukawa couplings through SM Higgs. We briefly discuss this possibility in the remainder of this section.

Once the Z_2 symmetry is discarded, one can have new non-diagonal terms in the RHN mass matrix. However, for simplicity we continue to choose a diagonal RHN mass matrix or the corresponding Yukawa coupling matrix Y_N. The newly introduced Yukawa couplings of N_1 to SM leptons can be written as

$$-\mathcal{L}_{\mathcal{Y}} \supset \sum_{\alpha=e,\mu,\tau} (Y_D)_{1\alpha} \overline{l_L}^{\alpha} \tilde{H} N_{R_1}, \tag{50}$$

This will generate mixing of N_1 with active neutrinos once the electroweak symmetry is broken. Using Casas–Ibarra parametrisation of Eq. (19) and using the form of complex orthogonal matrix given in Eq. (20), the Yukawa coupling of N_1 with leptons can be expressed as

$$(Y_D)^T_{1\alpha} = \frac{\sqrt{2}}{v} \begin{pmatrix} 0.146\sqrt{m_3}\sqrt{M_{N_1}} \sin\gamma' \\ 0.648\sqrt{m_3}\sqrt{M_{N_1}} \sin\gamma' \\ 0.746\sqrt{m_3}\sqrt{M_{N_1}} \sin\gamma' \end{pmatrix} \tag{51}$$

where γ' is a complex angle and m_3 the heaviest active neutrino mass with normal ordering. In deriving this, we fix Dirac CP phase to be zero[5] and also considered the lightest active neutrino as massless. The requirement of the lightest active neutrino mass to be vanishingly small arises due to tiny Yukawa couplings of N_1 to leptons for being a FIMP DM.

[5] Although recent experimental results hint towards a non-vanishing leptonic CP phase [39], it does not affect our analysis significantly.

We define the mixing of sterile N_1 with i^{th} active neutrino by:

$$\tan\delta_i = -\frac{\sqrt{2}\,(Y_D)_{1i}\,v}{M_{N_1}}. \tag{52}$$

For simplicity, we redefine $\delta_1 = \delta$ and the relation between δ and $\delta_{2,3}$ can be easily found using Eq. (51). Owing to this tiny but non-zero mixing, N_1 can now interact with SM bath directly without relying upon Z_{BL} or H_2 mediation considered earlier in Z_2 symmetric scenario. For example, $W^{\pm}$ boson can directly decay to N_1 through $W^{\pm} \to N_1\alpha^{\pm}$, $\alpha \equiv (e, \mu, \tau)$ if kinematically allowed. The contribution from annihilation processes continues to be sub-dominant like before. The evolution of DM comoving number density is governed by

$$\frac{dY_{\rm DM}}{dz} = \frac{2M_P}{1.66M^2_{H_1}} \frac{z\sqrt{g_*(z)}}{g_{*s}(z)} \Big(\langle\Gamma_{H_1\to\nu_\alpha N_1}\rangle(Y^{\rm eq}) + \langle\Gamma_{W^{\pm}\to e^{\pm}N_1}\rangle(Y^{\rm eq}) \Big), \tag{53}$$

where we have considered only the most dominant decay modes and completely ignored the annihilation processes which are sub-dominant. Decay channels with more than one N_1 in final state will be suppressed due to higher powers of tiny mixing δ. Once we obtain $Y_{\rm DM}$, it is simple to compute the relic density of the DM using Eq. (49) discussed earlier. It turns out that the DM relic abundance is primarily determined by the decay of $W^{\pm}$ (with other RHNs very heavy compared to DM) which further depends crucially on the mixing parameter δ. In Fig. 16, we show the contour for the observed relic abundance in $M_{N_1} - \delta$ plane. The figure shows the dependence of relic abundance on both DM mass the mixing δ with lower M_{N_1} requiring larger δ, as expected. The magnitude of δ (Y_{1e}) is required to be extremely small to generate correct order of DM relic abundance. Such a tiny Yukawa element can be obtained by suitable value of free parameter γ' in Eq. (19). While generating figure 16, we assume $M_{Z_{BL}} = 10^4$ GeV, $M_{N_2} = 10^9$ GeV, $M_{N_3} = 3 \times 10^9$ GeV and $\lambda_2 = 4.35 \times 10^{-10}$ (corresponding to $\xi = 1$) with $\lambda_3 = 10^{-10}$, $g_{BL} = 10^{-12}$ at inflationary energy scale. For these set of values, H_2 remains out of equilibrium after reheating. We have also confirmed that the contour for the observed relic abundance remains more or less same with

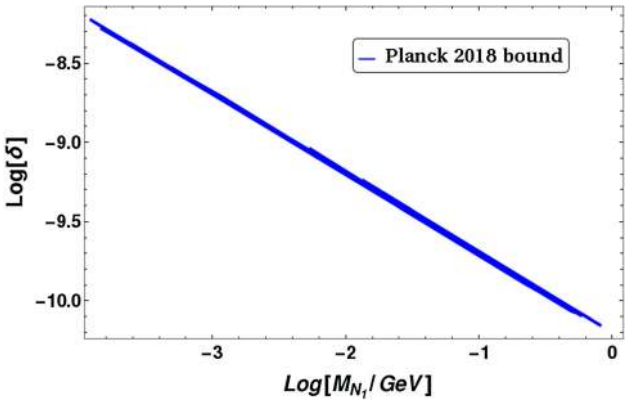

Fig. 16 Contour for observed relic abundance in $\delta - M_{N_1}$ plane considering H_2 to be out of equilibrium and DM production from tree level decay of $W^{\pm}$ boson

different orders of of λ_2, λ_3 and g_{BL} provided $\lambda_3 \lesssim \lambda_2$ and $M_{H_2} > T_R$. This is expected since here DM gets produced from W boson decay which stays in thermal equilibrium.

It is to be noted that, unlike the WIMP scenario, we are not performing a complete scan of parameter space for FIMP which can be found elsewhere. We have considered two possibilities based on inflation mass being smaller or larger compared to reheat temperature and showed that required FIMP DM abundance can be successfully produced in both the scenarios. In the case where inflation mass is larger compared to reheat temperature so that it is not present in the thermal bath afterwards, we find that the correct FIMP abundance can be produced only when we discard the Z_2 stabilising symmetry of DM and allow for more possibilities of its production from SM bath to open up. It is relevant to note here that such removal of Z_2 symmetry could produce extra relic through Dodelson–Widrow mechanism [116]. However, considering the smallness of δ we have obtained to satisfy the observed relic limit, this effect is expected to be negligible. On the other hand, such long-lived dark matter can have very interesting consequences at indirect detection experiments, which have been summarised in the review article [117].

6 Leptogenesis

In this section, we briefly discuss the possibilities of generating the observed baryon asymmetry of the universe through leptogenesis. Since the lightest right handed neutrino is our DM candidate, the required lepton asymmetry can be generated only by the out of equilibrium decays of heavier right handed neutrinos $N_{2,3}$. Usually, in such type I seesaw framework, the requirement of producing the correct lepton asymmetry pushes the scale of right handed neutrinos to a very high scale $M > 10^9$ GeV, known as the Davidson–Ibarra bound [118] of high scale or vanilla leptogenesis. For right handed neutrino masses lower than this, say around TeV scale, it is still possible to generate correct lepton asymmetry by resorting to a resonant enhancement of the CP-asymmetry with a quasi-degenerate right handed neutrino spectrum [119,120], known as resonant leptogenesis. In both vanilla as well as resonant leptogenesis, it is assumed that right handed neutrinos were produced thermally in the early universe along with other SM particles. For earlier works on thermal leptogenesis in gauged $B - L$ model, please refer to [121–123] and references therein. Due to the presence of gauge interactions of right handed neutrinos in this model, there exist additional washout processes erasing the created asymmetry which leads to tight constraints on such $B - L$ gauge sectors, specially for low scale leptogenesis. Since we find thermal DM to be disfavoured in our model, we therefore do not discuss thermal leptogenesis any further. Also, thermal leptogenesis is not affected much by inflationary dynamics at high scale. It is of course possible to realise thermal leptogenesis and non-thermal DM in this model, but we focus mainly on non-thermal leptogenesis due to its connection to inflation as well as reheat temperature as discussed below. In fact, thermal vanilla leptogenesis is not possible in our setup as the predicted values of reheat temperature (for $g_{BL}, \Sigma_N^4 \ll \lambda_2^2$) discussed earlier (see Fig. 8) falls below the Davidson–Ibarra limit on scale of such leptogenesis. This motivates us to discuss non-thermal leptogenesis in this section.

The scenario of non-thermal leptogenesis [48–56] arises when the reheat temperature after inflation is lower than the masses of right handed neutrinos. Thus, although the right handed neutrinos can be produced due to the decay of inflation, they cannot reach thermal equilibrium with the SM particles due to insufficient reheat temperature. The non-equilibrium abundance of right handed neutrinos will be purely decided by their couplings to inflation which will affect the final CP asymmetry generated by subsequent decays of right handed neutrinos. Since inflation also has to decay into other SM bath particles reproducing a radiation dominated universe, one has to solve coupled Boltzmann equations involving inflation, right handed neutrinos and SM radiation. However, for simplicity, we assume that the decay width of $N_{2,3}$'s ($\Gamma_{N_{2,3}}$) to be larger than that of the inflation (Γ_{H_2}) so that decays of $N_{2,3}$ to SM particles can be instantaneous [54]. This allows us to retain the same reheating description (from inflation decay only) discussed earlier. Thus, the right handed neutrinos produced from inflation decay turns non-relativistic and decays to SM leptons and Higgs instantaneously. The CP asymmetry generated by N_i decays, following the notations of [53], can be formulated as

$$\epsilon_A = \sum_{i=2}^{3} \frac{\Gamma(N_i \to H + l_L) - \Gamma(N_i \to H^\dagger + \overline{l_L})}{\Gamma(N_i \to H + l_L) + \Gamma(N_i \to H^\dagger + \overline{l_L})}$$
$$= \epsilon_A^2 + \epsilon_A^3 \tag{54}$$
$$= \frac{1}{8\pi} \frac{\mathrm{Im}\left[\left(Y_D Y_D^\dagger\right)_{23}\right]^2}{\left(Y_D Y_D^\dagger\right)_{22}} \mathcal{G}\left(\frac{M_{N_3}}{M_{N_2}}\right)$$
$$+ \frac{1}{8\pi} \frac{\mathrm{Im}\left[\left(Y_D Y_D^\dagger\right)_{32}\right]^2}{\left(Y_D Y_D^\dagger\right)_{33}} \mathcal{G}\left(\frac{M_{N_2}}{M_{N_3}}\right), \tag{55}$$

where the first and second terms in Eq. (55) are the individual contributions of N_2 and N_3 respectively. The loop function $\mathcal{G}(x)$ containing both self-energy and vertex corrections is defined as

$$\mathcal{G}(x) = -x\left[\frac{2}{x^2-1} + \ln\left(1 + \frac{1}{x^2}\right)\right]. \tag{56}$$

Once the CP asymmetry parameter is calculated, the comoving lepton asymmetry (ratio of excess of leptons over antileptons and entropy) can be calculated as

$$\frac{n_L}{s} = \epsilon_A^2 \mathrm{Br}_2 \frac{3T_R}{2M_{H_2}} + \epsilon_A^3 \mathrm{Br}_3 \frac{3T_R}{2M_{H_2}}, \tag{57}$$

where Br_i represents the branching ratio of the inflation decay to N_i. Finally, the baryon asymmetry generated through the standard sphaleron conversion processes is given by

$$Y_B = \frac{n_B - n_{\bar{B}}}{s} = -\frac{28}{79}\frac{n_L}{s}. \tag{58}$$

We have used the Casas–Ibarra parametrisation of Y_D as given by Eq. (19). Since lepton asymmetry gets generated from N_2 and N_3 decays, the complex angle γ in Eq. (20) is an important parameter to be tuned appropriately. Note that there is not much freedom to choose γ' as it appears in FIMP DM coupling discussed earlier. We consider it to be vanishingly small for leptogenesis discussions. As in the preceding analysis, here also we consider $M_{N_3} = 3 \times M_{N_2}$. Thus it is expected that N_2 will dominantly contribute to the baryon asymmetry.

It is to be noted that in the present scenario the inflation has several other decay modes, in addition to its decay into RHNs. Thus it is difficult to generate the observed amount of baryon asymmetry where the inflation decays to RHNs are subdominant or $\mathrm{Br}_{\phi \to N_{2,3} N_{2,3}} \ll 1$. So, one needs to find the parameter space where the branching ratio of inflation to RHNs as well as the CP asymmetry from RHN decay can be large enough to satisfy the requirement of baryon asymmetry. The decay widths of RHNs N_2 and N_3 into SM leptons and Higgs depend on the strength of Yukawa couplings as defined in Eq. (19). Below we provide the structure of $Y_{D_{2i}}$ and $Y_{D_{3i}}$ (see Eq. (51) for $Y_{D_{1i}}$) where we have considered best fit values of light neutrino mass parameters with vanishing Dirac CP phase[6] and vanishing lightest active neutrino mass (normal ordering).

$$Y_{D_{2,i}}^T = \frac{\sqrt{2}}{v} \begin{pmatrix} 0.56\sqrt{m_2}\sqrt{M_{N_2}} \cos\gamma + 0.146\sqrt{m_3}\sqrt{M_{N_3}} \cos\gamma' \sin\gamma \\ 0.56\sqrt{m_2}\sqrt{M_{N_2}} \cos\gamma + 0.648\sqrt{m_3}\sqrt{M_{N_3}} \cos\gamma' \sin\gamma \\ -0.60\sqrt{m_2}\sqrt{M_{N_2}} \cos\gamma + 0.746\sqrt{m_3}\sqrt{M_{N_3}} \cos\gamma' \sin\gamma \end{pmatrix} \tag{59}$$

$$Y_{D_{3,i}}^T = \frac{\sqrt{2}}{v} \begin{pmatrix} 0.146\sqrt{m_3}\sqrt{M_{N_3}} \cos\gamma \cos\gamma' - 0.56\sqrt{m_2}\sqrt{M_{N_3}} \sin\gamma \\ 0.648\sqrt{m_3}\sqrt{M_{N_3}} \cos\gamma \cos\gamma' - 0.56\sqrt{m_2}\sqrt{M_{N_3}} \sin\gamma \\ 0.746\sqrt{m_3}\sqrt{M_{N_3}} \cos\gamma \cos\gamma' + 0.60\sqrt{m_2}\sqrt{M_{N_3}} \sin\gamma \end{pmatrix} \tag{60}$$

In Fig. 17, we show the allowed region which satisfies the bound on Y_B in $M_{H_2} - T_R$ plane for two different sets of complex angle γ considering $M_{N_2} = 10^9$ GeV. We vary g_{BL} and λ_2 in specified ranges mentioned in the figure. The regions labelled as $M_{N_2} < T_R$ and $M_{H_2} < 2M_{N_2}$ in magenta and yellow colours respectively are outside the regime of non-thermal leptogenesis discussed here. Similar plot is shown in Fig. 18 considering slightly higher scale of leptogenesis ($M_{N_2} = 10^{10}$ GeV) where the allowed region gets enhanced, as expected. In preparing both the figures we have taken $\lambda_3 \sim \mathcal{O}(10^{-15})$, such that the $\mathrm{Br}_{\phi \to N_{2,3} N_{2,3}}$ does not turn very small due to other decay modes of inflation which depend upon λ_3 or scalar mixing. We have also confirmed that corresponding to our choices of γ, the condition $\Gamma_{N_{2,3}} \gg \Gamma_{H_2}$ is satisfied, a requirement for validating the simplistic approach adopted here.

7 Conclusion

To summarise, we have studied the very popular gauged $B - L$ extension of the standard model by restricting ourselves to the minimal possible framework from the requirement of triangle anomaly cancellation, desired gauge symmetry breaking and origin of light neutrino mass. We particularly

[6] Even if we take non-vanishing Dirac CP phase, as suggested by recent experiment [39], it does not appear in the calculation of lepton asymmetry in unflavoured regime.

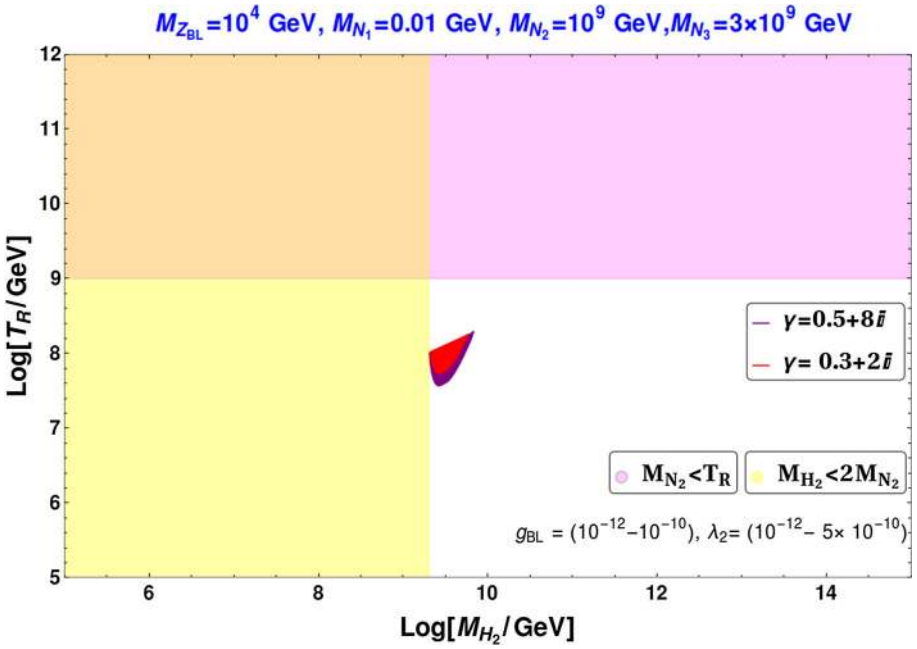

Fig. 17 Region allowed by the observed baryon asymmetry in $M_{H_2} - T_R$ plane by varying g_{BL}, λ_2 and angle γ considering $M_{N_2} = 10^9$ GeV. We also include the essential conditions to realize the non thermal leptogenesis such as $M_{N_2} > T_R$, $M_{H_2} > 2M_{N_2}$ in the figure

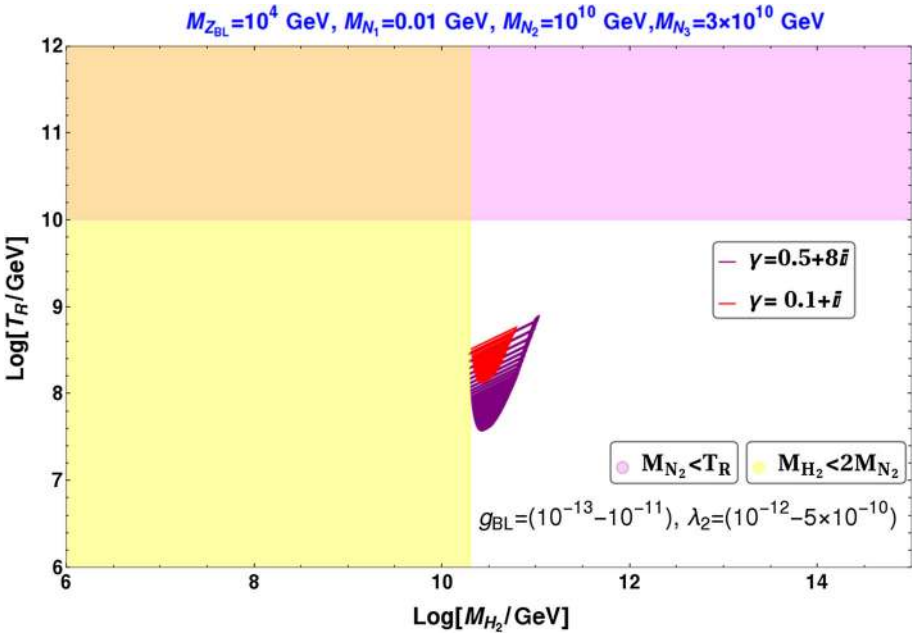

Fig. 18 Region allowed by the observed baryon asymmetry in $M_{H_2} - T_R$ plane by varying g_{BL}, λ_2 and angle γ considering $M_{N_2} = 10^{10}$ GeV. We also include the essential conditions to realise the non thermal leptogenesis such as $M_{N_2} > T_R$, $M_{H_2} > 2M_{N_2}$ in the figure

focus on the possibility of singlet scalar field responsible for breaking $B - L$ gauge symmetry spontaneously to also drive successful inflation in agreement with Planck 2018 data and its implications for dark matter and leptogenesis. While the lightest right handed neutrino is considered to be the DM candidate, the heavier two right handed neutrinos generate light neutrino masses through type I seesaw mechanism and also generate the required lepton asymmetry via their out of equilibrium decays. We first show that the requirement of successful inflationary phase tightly constrains the scalar and gauge sector couplings of the model. To be more precise, the requirement of stability of the inflationary potential puts an upper bound on $B - L$ gauge coupling along with inflation couplings to SM Higgs as well as right handed neutrinos. Since WIMP type DM in this model primarily interacts with the SM particles via $B - L$ gauge or singlet scalar (via its mixing with SM Higgs), the bounds derived from inflation on couplings and masses involved in these portals make WIMP annihilations inefficient. The parameter space where WIMP abundance satisfies the Planck 2018 data on DM abundance along with inflationary requirements, gets ruled out by LHC data on dilepton searches. This led to our first main conclusion that thermal DM is disfavoured in such scenario. We then considered the possibility of non-thermal DM by considering

two different broad scenarios related to the interplay of inflation mass and reheat temperature. We show that in both the scenarios correct FIMP abundance can be produced. We find that for a scenario where inflation is not part of the thermal bath after reheating, the required FIMP relic can be produced only if it is allowed to couple to SM leptons opening up several production channels from the SM bath. Such a scenario does not require any additional Z_2 symmetry considered for stabilising WIMP type DM and also have interesting consequences for indirect detection experiments due to possible decays into photons ranging from X-ray to gamma rays.

We then briefly discuss the possibility of leptogenesis by focusing primarily on non-thermal leptogenesis which is very much sensitive to the details of inflation. While resonant leptogenesis is still a viable option, thermal vanilla leptogenesis is not possible due to low reheat temperature predicted in our scenario. We find that inflationary requirements tightly constrain the scenario of non-thermal leptogenesis, precisely due to the same reason behind constraining or disfavouring WIMP type DM mentioned earlier. We show the possibility of producing observed baryon asymmetry from non-thermal leptogenesis for benchmark choices of some parameters while varying others and also show that the same parameters are also consistent with successful inflation, stability of inflation potential, FIMP DM abundance, neutrino mass apart from other experimental limits. Since the model is very minimal, it remains very predictive, specially when the requirements of correct neutrino mass, DM abundance, baryon asymmetry along with successful inflation are to be met with. Future data from all these frontiers should be able to restrict the model parameters to even stricter ranges while ruling out some of the possibilities.

Before we end, let us briefly comment on the fate of electroweak vacuum in view of our proposed inflationary scenario. During inflation, quantum fluctuations of the Higgs field are developed with amplitude proportional to the Hubble parameter during inflation $\sim H_{\rm Inf}$. This could be dangerous since the electroweak vacuum in the SM is metastable [124–127] and it is expected to remain same in our framework as well due to the small mixing angle between SM Higgs and singlet scalar. Usually in large scale inflation models, $H_{\rm Inf}$ turns bigger than the instability scale of the SM Higgs vacuum ($\sim 10^9$ GeV [124]) and therefore, during inflation, the Higgs field can cross the potential barrier towards the unbounded part [128]. This serious drawback of large scale inflation model can be easily avoided by introduction of inflation-Higgs quartic coupling. In that case, due to super-Planckian value of inflation field, the Higgs field acquires inflation dependent effective mass during inflation which becomes larger than the Hubble scale. Then, the quantum fluctuations of the Higgs field can be ignored. This holds in our analysis as well. However, some studies [129–131] have shown that the stability of the electroweak vacuum is essential even after inflation as oscillation phase of the inflation could trigger resonant enhancement of the Higgs fluctuations. Addressing the post inflationary Higgs instability is beyond the scope of our present work and introduction of additional degree of freedom in form of a scalar field may be useful to ensure this (see Ref. [131], for example). We leave such studies with next to minimal extension of the present model to future works.

Acknowledgements DB acknowledges the support from Early Career Research Award from DST-SERB, Government of India (reference number: ECR/2017/001873). SJD would like to thank Dibyendu Nanda and Devabrat Mahanta for some productive discussions. AKS is thankful to Rome Samanta for some useful discussions during WHEPP 2019. AKS also acknowledges PRL for providing postdoctoral research fellowship.

Data Availability Statement This manuscript has no associated data or the data will not be deposited. [Authors' comment: The present work offers a theoretical study of the different scenarios as discussed. All the figures are for the demonstration purpose and produced from simple stimulations without utilizing any actual data.]

Funded by SCOAP[3].

Appendix A: RGE equations

Here we present the complete set of RGEs at one loop level for the minimal B-L model:

$$\beta_{\lambda_1} = 24\lambda_1^2 + \lambda_3^2 - 6Y_D^4 + \frac{9}{8}g_1^4 + \frac{3}{8}g_2^4 + \frac{3}{4}g_1^2 g_2^2 + 12\lambda_1 Y_D^2 - 9\lambda_1 g_1^2 - 3\lambda_1 g_2^2 \tag{A1}$$

$$\beta_{\lambda_3} = \lambda_3\left(3\lambda_1 + 2\lambda_2 + \lambda_3 + \frac{3}{2}Y_D^2 - \frac{9}{8}g_1^2 - \frac{3}{8}g_2^2 + \Sigma_N^2 - 6g_{BL}^2\right) \tag{A2}$$

$$\beta_{g_s} = -7g_s^3 \beta_{g_1} = -\frac{19}{6}g_1^3 \tag{A3}$$

$$\beta_{g_2} = \frac{41}{6}g_2^3 \tag{A4}$$

$$\beta_{Y_D} = Y_D\left(\frac{9}{2}Y_D^2 - 8g_s^2 - \frac{9}{4}g_1^2 - \frac{17}{12}g_2^2 - \frac{2}{3}g_{BL}^2\right). \tag{A5}$$

where g_s, g_1 and g_2 represent the $SU(3)_C$, $SU(2)_L$ and $U(1)_Y$ gauge couplings respectively.

References

1. WMAP collaboration, E. Komatsu et al., Seven-Year Wilkinson Microwave Anisotropy Probe (WMAP) Observations: cosmological interpretation, Astrophys. J. Suppl. **192**, 18 (2011). arXiv:1001.4538
2. PLANCK collaboration, Y. Akrami et al., Planck 2018 results. X. Constraints on inflation (2018). arXiv:1807.06211
3. PLANCK collaboration, N. Aghanim et al., Planck 2018 results. VI. Cosmological parameters (2018). arXiv:1807.06209
4. A.H. Guth, The inflationary universe: a possible solution to the horizon and flatness problems. Phys. Rev. D **23**, 347 (1981)
5. A.A. Starobinsky, A new type of isotropic cosmological models without singularity. Phys. Lett. B **91**, 99 (1980)
6. A.D. Linde, A new inflationary universe scenario: a possible solution of the horizon, flatness, homogeneity, isotropy and primordial monopole problems. Phys. Lett. **108B**, 389 (1982)
7. A. Mazumdar, J. Rocher, Particle physics models of inflation and curvaton scenarios. Phys. Rept. **497**, 85 (2011). arXiv:1001.0993
8. A.D. Linde, Chaotic inflation. Phys. Lett. **129B**, 177 (1983)
9. J. Martin, C. Ringeval, V. Vennin, Encyclopedia Inflationaris. Phys. Dark Univ. **5–6**, 75 (2014). arXiv:1303.3787
10. K. Harigaya, M. Ibe, M. Kawasaki, T.T. Yanagida, Revisiting the minimal chaotic inflation model. Phys. Lett. B **756**, 113 (2016). arXiv:1506.05250
11. A.K. Saha, A. Sil, Higgs Vacuum stability and modified chaotic inflation. Phys. Lett. B **765**, 244 (2017). arXiv:1608.04919
12. D. Borah, D. Nanda, A.K. Saha, Common origin of modified chaotic inflation, non thermal dark matter and Dirac neutrino mass (2019). arXiv:1904.04840
13. F.L. Bezrukov, M. Shaposhnikov, The Standard Model Higgs boson as the inflation. Phys. Lett. B **659**, 703 (2008). arXiv:0710.3755
14. F. Bezrukov, A. Magnin, M. Shaposhnikov, S. Sibiryakov, Higgs inflation: consistency and generalisations. JHEP **01**, 016 (2011). arXiv:1008.5157
15. M. Sher, Electroweak Higgs potentials and vacuum stability. Phys. Rept. **179**, 273 (1989)
16. R.N. Lerner, J. McDonald, Higgs inflation and naturalness. JCAP **1004**, 015 (2010). arXiv:0912.5463
17. C. Pallis, Q. Shafi, Gravity waves from non-minimal quadratic inflation. JCAP **1503**, 023 (2015). arXiv:1412.3757
18. N. Kaewkhao, B. Gumjudpai, Cosmology of non-minimal derivative coupling to gravity in Palatini formalism and its chaotic inflation. Phys. Dark Univ. **20**, 20 (2018). arXiv:1608.04014
19. T. Tenkanen, Resurrecting quadratic inflation with a non-minimal coupling to gravity. JCAP **12**, 001 (2017). arXiv:1710.02758
20. M. Shokri, F. Renzi, A. Melchiorri, Cosmic Microwave Background constraints on non-minimal couplings in inflationary models with power law potentials. Phys. Dark Univ. **24**, 100297 (2019). arXiv:1905.00649
21. PARTICLE DATA GROUP collaboration, M. Tanabashi et al., Review of particle physics. Phys. Rev. D **98**, 030001 (2018)
22. F. Zwicky, Die Rotverschiebung von extragalaktischen Nebeln. Helv. Phys. Acta **6**, 110 (1933)
23. V.C. Rubin, W.K. Ford Jr., Rotation of the andromeda nebula from a spectroscopic survey of emission regions. Astrophys. J. **159**, 379 (1970)
24. D. Clowe, M. Bradac, A.H. Gonzalez, M. Markevitch, S.W. Randall, C. Jones et al., A direct empirical proof of the existence of dark matter. Astrophys. J. **648**, L109 (2006). arXiv:astro-ph/0608407
25. E.W. Kolb, M.S. Turner, The early universe. Front. Phys. **69**, 1 (1990)
26. LUX collaboration, D.S. Akerib et al., Results from a search for dark matter in the complete LUX exposure, Phys. Rev. Lett. **118**, 021303 (2017). arXiv:1608.07648
27. PANDAX- II collaboration, A. Tan et al., Dark matter results from first 98.7 days of data from the PandaX-II experiment. Phys. Rev. Lett. **117**, 121303 (2016). arXiv:1607.07400
28. PANDAX- II collaboration, X. Cui et al., Dark matter results from 54-ton-day exposure of PandaX-II Experiment (2017). arXiv:1708.06917
29. XENON collaboration, E. Aprile et al., First dark matter search results from the XENON1T Experiment (2017). arXiv:1705.06655
30. E. Aprile et al., Dark Matter Search results from a one tonne $\times$ year exposure of XENON1T (2018). arXiv:1805.12562
31. L.J. Hall, K. Jedamzik, J. March-Russell, S.M. West, Freeze-in production of FIMP Dark Matter. JHEP **03**, 080 (2010). arXiv:0911.1120
32. N. Bernal, M. Heikinheimo, T. Tenkanen, K. Tuominen, V. Vaskonen, The Dawn of FIMP dark matter: a review of models and constraints. Int. J. Mod. Phys. A **32**, 1730023 (2017). arXiv:1706.07442
33. A.D. Sakharov, Violation of CP Invariance, C asymmetry, and baryon asymmetry of the universe. Pisma Zh. Eksp. Teor. Fiz. **5**, 32 (1967)
34. S. Weinberg, Cosmological production of Baryons. Phys. Rev. Lett. **42**, 850 (1979)
35. E.W. Kolb, S. Wolfram, Baryon number generation in the early universe. Nucl. Phys. B **172**, 224 (1980)
36. M. Fukugita, T. Yanagida, Baryogenesis without grand unification. Phys. Lett. B **174**, 45 (1986)
37. V.A. Kuzmin, V.A. Rubakov, M.E. Shaposhnikov, On the anomalous electroweak baryon number nonconservation in the early universe. Phys. Lett. **155B**, 36 (1985)
38. I. Esteban, M.C. Gonzalez-Garcia, A. Hernandez-Cabezudo, M. Maltoni, T. Schwetz, Global analysis of three-flavour neutrino oscillations: synergies and tensions in the determination of $\theta_2 3$, $\delta_C P$, and the mass ordering. JHEP **01**, 106 (2019). arXiv:1811.05487
39. T2K collaboration, K. Abe et al., Constraint on the matter–antimatter symmetry-violating phase in neutrino oscillations. Nature **580**, 339 (2020). arXiv:1910.03887
40. P. Minkowski, $\mu \to e\gamma$ at a Rate of One Out of 10^9 Muon Decays? Phys. Lett. B **67**, 421 (1977)
41. R.N. Mohapatra, G. Senjanovic, Neutrino mass and spontaneous parity violation. Phys. Rev. Lett. **44**, 912 (1980)
42. T. Yanagida, Horizontal symmetry and masses of neutrinos. Conf. Proc. **C7902131**, 95 (1979)
43. M. Gell-Mann, P. Ramond, R. Slansky, Complex spinors and unified theories. Conf. Proc. **C790927**, 315 (1979). arXiv:1306.4669
44. S.L. Glashow, The future of elementary particle physics. NATO Sci. Ser. B **61**, 687 (1980)
45. J. Schechter, J.W.F. Valle, Neutrino masses in SU(2) x U(1) theories. Phys. Rev. D **22**, 2227 (1980)
46. P. Di Bari, Seesaw geometry and leptogenesis. Nucl. Phys. B **727**, 318 (2005). arXiv:hep-ph/0502082
47. D. Mahanta, D. Borah, Fermion dark matter with N_2 leptogenesis in minimal scotogenic model. JCAP **11**, 021 (2019). arXiv:1906.03577
48. G. Lazarides, Q. Shafi, Origin of matter in the inflationary cosmology. Phys. Lett. B **258**, 305 (1991)
49. G. Giudice, M. Peloso, A. Riotto, I. Tkachev, Production of massive fermions at preheating and leptogenesis. JHEP **08**, 014 (1999). arXiv:hep-ph/9905242
50. T. Asaka, K. Hamaguchi, M. Kawasaki, T. Yanagida, Leptogenesis in inflation decay. Phys. Lett. B **464**, 12 (1999). arXiv:hep-ph/9906366

51. T. Asaka, K. Hamaguchi, M. Kawasaki, T. Yanagida, Leptogenesis in inflationary universe. Phys. Rev. D **61**, 083512 (2000). arXiv:hep-ph/9907559
52. M. Fujii, K. Hamaguchi, T. Yanagida, Leptogenesis with almost degenerate majorana neutrinos. Phys. Rev. D **65**, 115012 (2002). arXiv:hep-ph/0202210
53. S. Pascoli, S. Petcov, C. Yaguna, Quasidegenerate neutrino mass spectrum, mu -> e + gamma decay and leptogenesis. Phys. Lett. B **564**, 241 (2003). arXiv:hep-ph/0301095
54. T. Asaka, H. Nielsen, Y. Takanishi, Nonthermal leptogenesis from the heavier Majorana neutrinos. Nucl. Phys. B **647**, 252 (2002). arXiv:hep-ph/0207023
55. G. Panotopoulos, Non-thermal leptogenesis and baryon asymmetry in different neutrino mass models. Phys. Lett. B **643**, 279 (2006). arXiv:hep-ph/0606127
56. F. Hahn-Woernle, M. Plumacher, Effects of reheating on leptogenesis. Nucl. Phys. B **806**, 68 (2009). arXiv:0801.3972
57. A. Davidson, $B?L$ as the fourth color within an $SU(2)_L \times U(1)_R \times U(1)$ model. Phys. Rev. D **20**, 776 (1979)
58. R.N. Mohapatra, R.E. Marshak, Local B-L symmetry of electroweak interactions, majorana neutrinos and neutron oscillations. Phys. Rev. Lett. **44**, 1316 (1980)
59. R.E. Marshak, R.N. Mohapatra, Quark–lepton symmetry and B-L as the U(1) generator of the electroweak symmetry group. Phys. Lett. **91B**, 222 (1980)
60. A. Masiero, J.F. Nieves, T. Yanagida, B^-l violating proton decay and late Cosmological Baryon production. Phys. Lett. **116B**, 11 (1982)
61. R.N. Mohapatra, G. Senjanovic, Spontaneous breaking of global B^-l symmetry and matter-antimatter oscillations in grand unified theories. Phys. Rev. D **27**, 254 (1983)
62. W. Buchmuller, C. Greub, P. Minkowski, Neutrino masses, neutral vector bosons and the scale of B-L breaking. Phys. Lett. B **267**, 395 (1991)
63. J.C. Montero, V. Pleitez, Gauging U(1) symmetries and the number of right-handed neutrinos. Phys. Lett. B **675**, 64 (2009). arXiv:0706.0473
64. W. Wang, Z.-L. Han, Radiative linear seesaw model, dark matter, and $U(1)_{B-L}$. Phys. Rev. D **92**, 095001 (2015). arXiv:1508.00706
65. S. Patra, W. Rodejohann, C.E. Yaguna, A new B–L model without right-handed neutrinos, JHEP **09**, 076 (2016). arXiv:1607.04029
66. D. Nanda, D. Borah, Common origin of neutrino mass and dark matter from anomaly cancellation requirements of a $U(1)_{B-L}$ model. Phys. Rev. D **96**, 115014 (2017). arXiv:1709.08417
67. N. Bernal, D. Restrepo, C. Yaguna, O. Zapata, Two-component dark matter and a massless neutrino in a new $B-L$ model (2018). arXiv:1808.03352
68. A. Biswas, D. Borah, D. Nanda, Type III Seesaw for neutrino masses in $U(1)_{B-L}$ model with multi-component dark matter (2019). arXiv:1908.04308
69. D. Nanda, D. Borah, Connecting light dirac neutrinos to a multi-component dark matter scenario in gauged $B-L$ Model (2019). arXiv:1911.04703
70. J.A. Casas, A. Ibarra, Oscillating neutrinos and muon -> e, gamma. Nucl. Phys. B **618**, 171 (2001). arXiv:hep-ph/0103065
71. A. Ibarra, G.G. Ross, Neutrino phenomenology: The Case of two right-handed neutrinos. Phys. Lett. B **591**, 285 (2004). arXiv:hep-ph/0312138
72. M. Carena, A. Daleo, B.A. Dobrescu, T.M.P. Tait, Z' gauge bosons at the Tevatron. Phys. Rev. D **70**, 093009 (2004). arXiv:hep-ph/0408098
73. G. Cacciapaglia, C. Csaki, G. Marandella, A. Strumia, The minimal set of electroweak precision parameters. Phys. Rev. D **74**, 033011 (2006). arXiv:hep-ph/0604111
74. ATLAS collaboration, M. Aaboud et al., Search for new high-mass phenomena in the dilepton final state using 36.1 fb^{-1} of proton-proton collision data at $\sqrt{s}$ = 13 TeV with the ATLAS detector. arXiv:1707.02424
75. ATLAS collaboration, G. Aad et al., Search for high-mass dilepton resonances using 139 fb^{-1} of pp collision data collected at $\sqrt{s}$ =13 TeV with the ATLAS detector. Phys. Lett. B **796**, 68 (2019). arXiv:1903.06248
76. CMS collaboration, A. M. Sirunyan et al., Search for high-mass resonances in dilepton final states in proton-proton collisions at $\sqrt{s}$ = 13 TeV. JHEP **06**, 120 (2018). arXiv:1803.06292
77. B. Barman, D. Borah, P. Ghosh, A.K. Saha, Flavoured gauge extension of singlet-doublet fermionic dark matter: neutrino mass, high scale validity and collider signatures (2019). arXiv:1907.10071
78. T. Robens, T. Stefaniak, Status of the Higgs singlet extension of the standard model after LHC Run 1. Eur. Phys. J. C **75**, 104 (2015). arXiv:1501.02234
79. G. Chalons, D. Lopez-Val, T. Robens, T. Stefaniak, The Higgs singlet extension at LHC Run 2. PoS **ICHEP2016**, 1180 (2016). arXiv:1611.03007
80. D. Lopez-Val, T. Robens, Δr and the W-boson mass in the singlet extension of the standard model. Phys. Rev. D **90**, 114018 (2014). arXiv:1406.1043
81. CMS collaboration, V. Khachatryan et al., Search for a Higgs boson in the mass range from 145 to 1000 GeV decaying to a pair of W or Z bosons. JHEP **10**, 144 (2015). arXiv:1504.00936
82. M.J. Strassler, K.M. Zurek, Discovering the Higgs through highly-displaced vertices. Phys. Lett. B **661**, 263 (2008). arXiv:hep-ph/0605193
83. ATLAS Collaboration, Search for invisible Higgs boson decays with vector boson fusion signatures with the ATLAS detector using an integrated luminosity of 139 fb^{-1}, ATLAS-CONF-2020-008 (2020)
84. N. Okada, M.U. Rehman, Q. Shafi, Non-minimal B-L inflation with observable gravity waves. Phys. Lett. B **701**, 520 (2011). arXiv:1102.4747
85. N. Okada, D. Raut, Running non-minimal inflation with stabilized inflation potential. Eur. Phys. J. C **77**, 247 (2017). arXiv:1509.04439
86. W. Buchmuller, V. Domcke, K. Schmitz, Spontaneous B-L breaking as the origin of the hot early universe. Nucl. Phys. B **862**, 587 (2012). arXiv:1202.6679
87. R. Allahverdi, B. Dutta, A. Mazumdar, Unifying inflation and dark matter with neutrino masses. Phys. Rev. Lett. **99**, 261301 (2007). arXiv:0708.3983
88. D. Kazanas, R. Mohapatra, S. Nasri, V. Teplitz, Neutrino mass, dark matter and inflation. Phys. Rev. D **70**, 033015 (2004). arXiv:hep-ph/0403291
89. P. Van Dong, D. Huong, D.A. Camargo, F.S. Queiroz, J.W. Valle, Asymmetric dark matter, inflation and leptogenesis from $B-L$ symmetry breaking. Phys. Rev. D **99**, 055040 (2019). arXiv:1805.08251
90. D. Borah, P.S.B. Dev, A. Kumar, TeV scale leptogenesis, inflation dark matter and neutrino mass in a scotogenic model. Phys. Rev. D **99**, 055012 (2019). arXiv:1810.03645
91. S. Capozziello, R. de Ritis, A.A. Marino, Some aspects of the cosmological conformal equivalence between 'Jordan frame' and 'Einstein frame'. Class. Quantum Gravity **14**, 3243 (1997). arXiv:gr-qc/9612053
92. D.I. Kaiser, Conformal transformations with multiple scalar fields. Phys. Rev. D **81**, 084044 (2010). arXiv:1003.1159
93. N. Okada, M.U. Rehman, Q. Shafi, Tensor to scalar ratio in non-minimal ϕ^4 inflation. Phys. Rev. D **82**, 043502 (2010). arXiv:1005.5161
94. R. Allahverdi, R. Brandenberger, F.-Y. Cyr-Racine, A. Mazumdar, Reheating in inflationary cosmology: theory and applications. Ann. Rev. Nucl. Part. Sci. **60**, 27 (2010). arXiv:1001.2600

95. A. Albrecht, P.J. Kofman, M.S. Turner, F. Wilczek, Reheating an inflationary universe. Phys. Rev. Lett. **48**, 1437 (1982)
96. L. Kofman, A. Linde, A.A. Starobinsky, Reheating after inflation. Phys. Rev. Lett. **73**, 3195–3198 (1994). arXiv:hep-th/9405187
97. P. Greene, L. Kofman, A. Linde, A.A. Starobinsky, Structure of resonance in preheating after inflation. Phys. Rev. D **56**, 6175–6192 (1997). arXiv:hep-ph/9705347
98. L. Kofman, A. Linde, A.A. Starobinsky, Towards the theory of reheating after inflation. Phys. Rev. D **56**, 3258–3295 (1997). arXiv:hep-ph/9704452
99. G. Felder, L. Kofman, A. Linde, Instant preheating. Phys. Rev. D **59**, 123523 (1999). arXiv:hep-ph/9812289
100. J. García-Bellido, D.G. Figueroa, J. Rubio, Preheating in the standard model with the Higgs-inflation coupled to gravity. Phys. Rev. D **79**, 063531 (2009). arXiv:0812.4624
101. D. Maity, P. Saha, (P)reheating after minimal Plateau Inflation and constraints from CMB. JCAP07, 018 (2019). arXiv:1811.11173
102. F. Bezrukov, D. Gorbunov, M. Shaposhnikov, On initial conditions for the Hot Big Bang. JCAP **0906**, 029 (2009). arXiv:0812.3622
103. P.F. de Salas, M. Lattanzi, G. Mangano, G. Miele, S. Pastor, O. Pisanti, Bounds on very low reheating scenarios after Planck. Phys. Rev. D **92**, 123534 (2015). arXiv:1511.00672
104. N. Okada, O. Seto, Higgs portal dark matter in the minimal gauged $U(1)_{B-L}$ model. Phys. Rev. D **82**, 023507 (2010). arXiv:1002.2525
105. T. Basak, T. Mondal, Constraining minimal $U(1)_{B-L}$ model from dark matter observations. Phys. Rev. D **89**, 063527 (2014). arXiv:1308.0023
106. N. Okada, S. Okada, Z'_{BL} portal dark matter and LHC Run-2 results. Phys. Rev. D **93**, 075003 (2016). arXiv:1601.07526
107. S. Okada, Z' Portal dark matter in the minimal $B-L$ Model. Adv. High Energy Phys. **2018**, 5340935 (2018). arXiv:1803.06793
108. M. Escudero, S.J. Witte, N. Rius, The dispirited case of gauged $U(1)_{B-L}$ dark matter. JHEP **08**, 190 (2018). arXiv:1806.02823
109. Y. Mambrini, The ZZ' kinetic mixing in the light of the recent direct and indirect dark matter searches. JCAP **07**, 009 (2011). arXiv:1104.4799
110. P. Gondolo, G. Gelmini, Cosmic abundances of stable particles: Improved analysis. Nucl. Phys. B **360**, 145 (1991)
111. A. Alloul, N.D. Christensen, C. Degrande, C. Duhr, B. Fuks, Feyn-Rules 2.0 - A complete toolbox for tree-level phenomenology. Comput. Phys. Commun. **185**, 2250 (2014). arXiv:1310.1921
112. G. Belanger, F. Boudjema, A. Pukhov, A. Semenov, micrOMEGAs 3: A program for calculating dark matter observables. Comput. Phys. Commun. **185**, 960 (2014). arXiv:1305.0237
113. A. Biswas, A. Gupta, Freeze-in production of sterile neutrino dark matter in $U(1)_{B-L}$ Model. JCAP **1609**, 044 (2016). arXiv:1607.01469
114. A. Biswas, A. Gupta, Calculation of momentum distribution function of a non-thermal fermionic dark matter. JCAP **1703**, 033 (2017). arXiv:1612.02793
115. R.N. Mohapatra, N. Okada, Freeze-in dark matter from a minimal B-L model and possible grand unification (2020). arXiv:2005.00365
116. S. Dodelson, L.M. Widrow, Phys. Rev. Lett. **72**, 17–20 (1994). https://doi.org/10.1103/PhysRevLett.72.17. arXiv:hep-ph/9303287 [hep-ph]
117. M. Drewes et al., A white paper on keV sterile neutrino dark matter. JCAP **1701**, 025 (2017). arXiv:1602.04816
118. S. Davidson, A. Ibarra, A Lower bound on the right-handed neutrino mass from leptogenesis. Phys. Lett. B **535**, 25 (2002). arXiv:hep-ph/0202239
119. A. Pilaftsis, T.E.J. Underwood, Resonant leptogenesis. Nucl. Phys. B **692**, 303 (2004). arXiv:hep-ph/0309342
120. P.S.B. Dev, M. Garny, J. Klaric, P. Millington, D. Teresi, Resonant enhancement in leptogenesis. Int. J. Mod. Phys. A **33**, 1842003 (2018). arXiv:1711.02863
121. S. Iso, N. Okada, Y. Orikasa, Resonant leptogenesis in the minimal B-L extended standard model at TeV. Phys. Rev. D **83**, 093011 (2011). arXiv:1011.4769
122. J. Heeck, D. Teresi, Leptogenesis and neutral gauge bosons. Phys. Rev. D **94**, 095024 (2016). arXiv:1609.03594
123. P.S.B. Dev, R.N. Mohapatra, Y. Zhang, Leptogenesis constraints on $B?L$ breaking Higgs boson in TeV scale seesaw models. JHEP **03**, 122 (2018). arXiv:1711.07634
124. G. Isidori, G. Ridolfi, A. Strumia, On the metastability of the standard model vacuum. Nucl. Phys. B **609**, 387 (2001). arXiv:hep-ph/0104016
125. D. Buttazzo, G. Degrassi, P.P. Giardino, G.F. Giudice, F. Sala, A. Salvio et al., Investigating the near-criticality of the Higgs boson. JHEP **12**, 089 (2013). arXiv:1307.3536
126. Y. Tang, Vacuum stability in the standard model. Mod. Phys. Lett. A **28**, 1330002 (2013). arXiv:1301.5812
127. L.A. Anchordoqui, I. Antoniadis, H. Goldberg, X. Huang, D. Lust, T.R. Taylor et al., Vacuum stability of standard model^{++}. JHEP **02**, 074 (2013). arXiv:1208.2821
128. A. Kobakhidze, A. Spencer-Smith, Electroweak vacuum (In)stability in an inflationary universe. Phys. Lett. B **722**, 130 (2013). arXiv:1301.2846
129. M. Herranen, T. Markkanen, S. Nurmi, A. Rajantie, Spacetime curvature and Higgs stability after inflation. Phys. Rev. Lett. **115**, 241301 (2015). arXiv:1506.04065
130. K. Kohri, H. Matsui, Higgs vacuum metastability in primordial inflation, preheating, and reheating. Phys. Rev. D **94**, 103509 (2016). arXiv:1602.02100
131. Y. Ema, K. Mukaida, K. Nakayama, Fate of electroweak vacuum during preheating. JCAP **10**, 043 (2016). arXiv:1602.00483